

AperTO - Archivio Istituzionale Open Access dell'Università di Torino

EPR Characterization and Reactivity of Surface-Localized Inorganic Radicals and Radical Ions

This is the author's manuscript

Original Citation:

Availability:

This version is available <http://hdl.handle.net/2318/82240> since

Terms of use:

Open Access

Anyone can freely access the full text of works made available as "Open Access". Works made available under a Creative Commons license can be used according to the terms and conditions of said license. Use of all other works requires consent of the right holder (author or publisher) if not exempted from copyright protection by the applicable law.

(Article begins on next page)



UNIVERSITÀ DEGLI STUDI DI TORINO

This is an author version of the contribution published on:

Questa è la versione dell'autore dell'opera:

[Chemical Reviews, Vol. 110, No. 3, 2010, DOI: 10.1021/cr800366v]

The definitive version is available at:

La versione definitiva è disponibile alla URL:

[<http://pubs.acs.org/journal/chreay>]

EPR Characterization and Reactivity of Surface Localized Inorganic Radicals and Radical Ions.

Mario Chiesa[†], Elio Giamello[†] and Michel Che[‡]

*Dipartimento di Chimica IFM and NIS, Università di Torino, 10125 Torino, Italy and
Laboratoire de Réactivité de Surface, UMR 7197-CNRS, Université Pierre et Marie Curie -
Paris 6 & Institut Universitaire de France.*

[†] Università di Torino

[‡] Université Pierre et Marie Curie - Paris 6

Contents

1. Introduction
2. Solid surfaces and paramagnetic species.
3. EPR techniques and surface chemistry.
 - 3.1. The spin-Hamiltonian formalism.
 - 3.2. Single crystal systems.
 - 3.3. Disordered systems.
4. Formation of radical species at solid surfaces.
 - 4.1. Mechanisms of radical generation at the surface.
 - 4.2. Chemical bonds between radicals and surfaces.
 - 4.3. Identification and reactivity of radical intermediates in heterogeneous catalysis.
 - 4.4. Radical intermediates in heterogeneous photocatalysis.
5. Experimental approaches in EPR of surface radical species.
 - 5.1. Paramagnetic probes of surface adsorption sites.
 - 5.2. Molecular motion of adsorbates on solid surfaces.
6. Main families of surface inorganic radicals: electronic configurations and geometry.
 - 6.1. Monoatomic species.
 - 6.2. Diatomic radical species.
 - 6.3. Triatomic, tetra-atomic and penta-atomic radical species.
7. Carbon containing inorganic radicals.
 - 7.1. The CO_2^- radical anion.
 - 7.2. Radicals generated from carbon monoxide.
 - 7.3. Carbon containing tetra-atomic and penta-atomic radicals.
8. Nitrogen containing radicals.
 - 8.1. The g tensor of 11-electron II radicals.
 - 8.2. Diatomic species: the radical anion of dinitrogen..
 - 8.3. Diatomic species. Nitric oxide a multipurpose surface probe.
 - 8.3.1. Cationic sites.
 - 8.3.2. Anionic sites.
 - 8.3.3 NO as a probe of surface transition metal ions.
 - 8.4. Nitrogen containing triatomic surface radicals.
 - 8.5. Nitrogen containing tetra-atomic and penta-atomic surface radicals.
9. Sulphur and chlorine containing radicals.
10. Conclusions.

1. Introduction.

Radicals are chemical species containing one or more unpaired electrons which generally react *via* electron pairing or electron transfer mechanisms. A charged radical is called a radical ion. Radical and radical ions are key species in a number of important chemical and biochemical processes ranging from atmospheric chemistry to polymerization and biochemistry.

For our purpose, radicals can be conveniently classified into two classes, organic and inorganic. While the former has been much investigated as intermediates in the context of reaction mechanisms, inorganic radicals have attracted the attention of the scientific community since the early days of radiation chemistry, because high energy irradiation often leads to the formation of radicals. In solid materials, the latter are often trapped in the bulk which makes their experimental investigation relatively easy. The book by Atkins and Symons,¹ published in 1967, represents the first thorough analysis of inorganic radicals available in the literature at the time.

Attention to inorganic radicals further increased with the development of the matrix isolation technique, for trapping, in basically inert matrices and often at low temperatures, a large number of inorganic radicals. A later book by Weltner, "*Magnetic Atoms and Molecules*" discusses this fascinating domain².

Although the field of surface-stabilized radicals is certainly more limited, in terms of the number of species isolated and characterised, it is however far richer from the chemical point of view. As a matter of fact, radicals can be stabilized by the surface *via* specific interactions on one hand and possess a different reactivity towards incoming adsorbates on the other hand. The importance of surface radicals owes much to that of surface phenomena which are involved in numerous fields such as heterogeneous catalysis, photochemistry, electrochemistry and corrosion phenomena, microelectronics, optoelectronics and, in general terms, nano-sciences and technology. Solids structured on a nanoscopic or mesoscopic scale bridge the gap between the atomic and macroscopic forms of matter and often possess very special chemical and physical properties caused by size and boundary effects. These very same effects are often responsible for enhanced chemical reactivity and formation and stabilization of uncommon radical species which are also important in structured solids with micro- and/or or meso-pores³. The elegant statement made by Wolfgang Pauli "*God created the solids, the devil their surfaces*", nicely summarises the problems concerned with sample preparation, low symmetry, and lack of experimental sensitivity which are commonly faced by researchers dealing with the characterisation of surfaces. While there are many methods to characterize an adsorbate, there are fewer which can give information at the molecular level on the adsorbate-surface system, in terms of interaction and structure. Electron Paramagnetic

Resonance (EPR) techniques have turned to be most powerful to achieve this goal, providing of course that the adsorbate-surface system be paramagnetic.

The present review intends to describe and classify the variety of inorganic radicals which are formed at oxide surfaces, emphasizing the importance of the structure-reactivity relationship and adsorbate-surface interaction. The surface can be that of small crystallites or the internal surface of a porous system accessible to molecules. Radical formation is not uncommon during chemical processes taking place at surfaces. Radicals are usually intermediates of complex processes like, for instance, an electrochemical process or a catalytic reaction. However, under particular experimental conditions (e.g. at temperatures lower than that of the reaction) they can be stable and directly observed. The quality of investigations on inorganic radicals has followed the development of EPR techniques which are most suitable to detect paramagnetic species and to unravel, often in great detail, their nature and their geometrical and electronic structure. It is therefore understandable that, rather often, experimental work on inorganic radical species relies exclusively on these experimental techniques.

A number of topics are not included in the present review. Firstly, surface organic radicals because their large number and particular features require a specific analysis. For an exhaustive account on this specific topic we refer the Reader to a review by Garcia and Roth.⁴ Secondly, transition elements compounds involved in interfacial coordination chemistry which have been the object of some specific recent reviews.^{5,6} The solid-solid interface is also not discussed, because the corresponding radicals are essentially not reactive. Furthermore we have to mention the family of surface oxygen radicals. Because of their importance in oxidation catalysis these radicals have been the subject of extensive reviews.^{7,8} We will therefore avoid, in the present paper, a systematic review of this field limiting ourselves to use recent examples to clarify important concepts concerning structure-reactivity relationship or to discuss adsorbate-surface interactions. Finally we have to mention the particular case of radicals generated at a solid-liquid interface and released in the liquid phase. In this case the direct detection of the radicals is often impossible and an indirect technique called spin trapping is used⁹ based on the addition of the reactive radical to a diamagnetic molecule (the trap). The reaction origins a stable paramagnetic adduct whose EPR spectrum bears information on the starting radical.¹⁰ Classification of this kind of spin trapped radicals in liquid phase is not among the purposes of the present review.

The present review paper is organized as follows. In Section 2, the importance of paramagnetic species in phenomena occurring at solid surfaces is outlined. Section 3 gives a brief survey of EPR techniques used to characterize the radicals. A description of the nature of surface inorganic radicals is reported in Section 4, with particular attention to their classification, to the

nature of their interaction with the surface and to the chemical mechanisms leading to their formation, while the role of EPR in surface chemistry and catalysis studies is dealt with in Section 5. In the following Sections (6-9), the main families of surface inorganic radicals are reviewed using a criterion based on their composition and number of valence electrons¹.

2. Paramagnetic species in solids and at surfaces.

In the field of surface science and heterogeneous catalysis, EPR techniques may be used to investigate i) either directly a radical, or ii) indirectly a diamagnetic system *via* a radical, often called *spin probe*. The latter is a molecule which, interacting with the surface, allows to monitor one of its properties (Section 8.3).

In the bulk of a solid or at its surface, different types of paramagnetic species can be present before and/or after adsorption of gas phase molecules (Figure 1). These can be related to the composition of the solid or derive from chemical reactivity in heterogeneous processes. Among the various elementary steps which initiate a surface chemical reaction, in fact, there are several cases involving the formation of species with unpaired electrons¹¹. This occurs for example in the case of electron transfer between solid and adsorbed molecules (oxidation catalysis, electrochemical processes), in that of hydrogen abstraction from a molecule (activation of alkanes) and in photocatalytic processes which are based on photo-induced charge separation and successive surface reaction of adsorbed molecules with either an electron or an hole.

In a catalytic system paramagnetic species can be found, prior any surface interaction with incoming molecules, in the bulk or at the surface of the solid. In both cases they are observed by EPR but only those located at surface are able to react with molecules in the gas phase or, alternatively, to broaden their EPR lines in the presence of a physisorbed paramagnetic gas like molecular oxygen, thus providing an easy method for distinguishing surface from bulk paramagnetic species. The suffix (surf) will be hereafter employed in chemical equations to distinguish species located at the surface from those in the bulk.

Far from being exhaustive and with an obvious degree of arbitrariness, Figure 1 illustrates some of the possible cases available at a gas-solid interface adopting as an example an oxide catalyst composed by M^{x+} and O^{2-} ions and containing a variety of paramagnetic centres in interaction with diamagnetic molecules of carbon monoxide from the gas phase. Prior to reaction paramagnetic centres (evidenced in yellow) are : a) bulk transition metal ions; b) surface transition metal ions; c) grafted transition metal ions; d) bulk paramagnetic defects (for example trapped

electrons or trapped holes); e) and f) surface localized defect centres (trapped electrons and holes respectively); g) metal clusters.

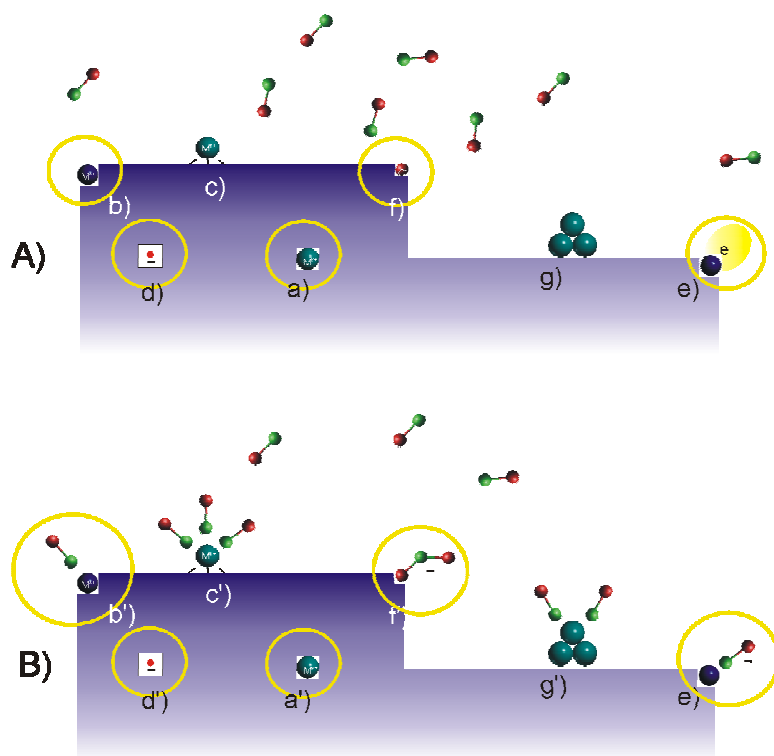


Figure 1 Illustration of typical situations present at a gas solid interface. A) Before reaction, B) After reaction. Yellow circle identify paramagnetic species (see text). Notice that a paramagnetic centre in (A) can be found “in” the bulk (a, d), “at” the surface when it belongs to the solid but is localized at the surface (b, e, f) or “on” the surface when it derives from chemical addition (c,g).

Reactivity involves surface centres only, which, in the examples shown in the Figure, maintain upon reaction their paramagnetic character (evidenced in green). Paramagnetic carbonyls (b', c') form after CO addition while the two surface defects are transformed in CO^- (e') and CO_2^- (f') radical ions respectively. The suffix (ads) will be hereafter employed in chemical equations to indicate a species adsorbed on the surface which does not contain atoms of the solid ($\text{CO}_{(\text{ads})}$, Figure 1 b') while the suffix (surf) will be adopted in the case of a species formed at the surface, containing one or more atoms belonging to the solid (Figure 1f' $\text{CO}_2^-_{(\text{surf})}$).

Although very schematic, Figure 1 conveys the idea that there exists a large variety of cases which can be investigated by EPR. In all these cases EPR is an instrumental tool as it can deeply probe those features of the molecular structure related to the unpaired electron charge distribution, thus providing detailed answers relative to the nature, structure, spatial distribution and dynamics of surface paramagnetic species. Modern surface chemistry is driven by the aim of understanding at

molecular level the chemical processes occurring at the surface. In this respect relevant fundamental questions concern the structure and reactivity of surfaces by themselves and of surfaces with atoms or molecules on them. In the same way the discovery of the basic mechanistic steps involved in surface reactivity and catalysis represents one of the most critical issues. These are the very questions that can be addressed (and answered) by EPR when paramagnetic species are involved.

3. EPR techniques and surface chemistry.

EPR techniques are, beyond any doubt, the reference techniques for detection of radicals and, in general, of paramagnetic species¹². In the field of surface radical species an advantage of this technique, beside its specificity, is its high sensitivity which allow the detection of species in concentrations well below a monolayer coverage. Surface species, in fact, are often formed in very small amounts during surface chemical processes and catalytic reactions. Review articles devoted to the applications of EPR to surface chemistry, and mainly oriented towards catalytic phenomena, have been already published.^{13,14, 15,16}

The conventional CW-EPR (Continuous Wave-Electron Paramagnetic Resonance) has been until now largely dominant in surface studies. In a CW-EPR experiment the substance under investigation interacts with a homogeneous magnetic field which is allowed to vary in a selected range and is irradiated by a continuous flow of microwaves at fixed frequency which, when resonance conditions are fulfilled entails a transition between two spin states. The microwave frequencies are usually classified in terms of bands. Commercially available bands range from 1 GHz (L band) till 94 GHz (W-band) as resumed in Table 1 which also gives, beside frequency, wavelength and photon energy. The X-band is the most commonly used and the CW-EPR spectra reported in the following are, except otherwise specified, recorded in X-band.

Following what was done in Nuclear Magnetic Resonance about forty years ago, pulsed methods were introduced in EPR recently. With the advent of commercial instruments, these techniques, based on irradiation by controlled pulses of microwaves, started to undergo rapid development and found wider applications. Continuous wave techniques include CW-EPR, ENDOR (Electron Nuclear Double Resonance) and HF-EPR (High Field Electron Paramagnetic Resonance) while, among the many pulsed methods,^{17, 18, 19} we can find FS-ESE (Field Swept Electron Spin Echo), ESEEM (Electron Spin Echo Envelope Modulation) or FT-ESR (Fourier Transform Electron Spin Resonance) and pulsed ENDOR. Pulsed EPR has been applied to surface chemistry mainly in the case of systems containing transition metal ions.^{20,21}

3.1. The spin-Hamiltonian formalism.

The EPR spectrum of a paramagnetic species can be described by the spin Hamiltonian (1) which defines the main energy terms as follows:

$$\mathcal{H} = \mathcal{H}_{\text{EZ}} + \mathcal{H}_{\text{F}} + \mathcal{H}_{\text{HFS}} + \mathcal{H}_{\text{NZ}} + \mathcal{H}_{\text{Q}} \quad (1)$$

The first term is the electronic Zeeman operator ($\mathcal{H}_{\text{EZ}} = \beta_{\text{e}} \mathbf{S} \cdot \mathbf{g} \cdot \mathbf{B}$) which accounts for the interaction of the electron spin \mathbf{S} with the external magnetic field \mathbf{B} , β_{e} being the Bohr magneton. The interaction is gauged by the \mathbf{g} tensor, a 3x3 matrix which, in general, can be reduced to its diagonal form. In this form all extradiagonal elements are zero and the principal elements g_{xx} , g_{yy} , g_{zz} are put into evidence, their values depending on the electronic structure (ground and excited states) of the paramagnetic species.

The fine structure term ($\mathcal{H}_{\text{F}} = \mathbf{S} \cdot \mathbf{D} \cdot \mathbf{S}$) describes the interaction between two or more unpaired electrons through the \mathbf{D} tensor. This term is zero in the case of $S=1/2$ i.e. for the vast majority of surface inorganic radicals.

The third term ($\mathcal{H}_{\text{HFS}} = \mathbf{S} \cdot \mathbf{A} \cdot \mathbf{I}$) is much more important in our case because it represents the hyperfine interaction between electron spin and nuclear spins. \mathbf{A} is the hyperfine tensor and \mathbf{I} is the nuclear spin vector. In CW-EPR the hyperfine interactions give rise to lines splitting in the spectrum (the hyperfine structure). $2I + 1$ lines are expected for the interaction of the electron spin with a nucleus having nuclear spin quantum number I . \mathbf{A} is composed of two main contributions, i.e. the isotropic Fermi contact term (a scalar arising from the finite probability of the electron being located at the position of the nucleus) and the anisotropic electron-nucleus dipolar coupling expressed by a matrix \mathbf{T} . The term hyperfine interaction is usually associated to the magnetic interaction between the unpaired electron of a given species and the nuclei belonging to the species itself. The same type of interaction which involves magnetic nuclei of the surrounding lattice is usually called super-hyperfine (shf) interaction. Its physical origin is of course the same as the hyperfine interaction and the elements of the shf tensors may give important information about the composition of the surface adsorption site, the local symmetry and the nature of the chemical bond.

The last two terms in equation (1) (representing the nuclear Zeeman energy and the nuclear quadrupolar energy respectively) are less important than the previous ones as they affect very weakly the EPR spectra.

The EPR tensors can be classified on the basis of their symmetry (for instance, an isotropic tensor has three equal principal components, an axial tensor has two components equal differing from the third) which in turn depends on the point symmetry of the paramagnetic centre. Radicals and, in general, paramagnetic species located at solid surfaces are submitted to some symmetry restrictions

(some of the point groups possible for molecular species are not permitted at the surface⁶) and often radicals with very reduced symmetry are observed. In the three most symmetric cases (isotropic, axial and rhombic tensors) the axes of \mathbf{g} and \mathbf{A} tensors coincide while in the other cases they do not. The structure of the EPR tensors and the relationships between EPR symmetry and point symmetry of the paramagnetic centre are gathered in Table 2²².

3.2 Single crystal systems.

The presence of tensors in all terms of equation (1) reflects the anisotropy of magnetic interactions. In pragmatic terms, this means that, when the paramagnetic system is located into a single crystal, the EPR signal changes according to the orientation of the crystal in the external magnetic field \mathbf{B} . In a classic CW-EPR spectrum (performed at constant microwave frequency and by sweeping the magnetic field) the values of the \mathbf{g} tensor elements determine the position of the resonant field B_{res} while those of \mathbf{A} determine the amplitude A of the hyperfine splitting. Both B_{res} and A depend on the orientations. In the following we consider a simple system of a doublet state ($S = 1/2$) with no magnetic nuclei ($I = 0$) and an axial \mathbf{g} matrix with $g_{\perp} > g_{\parallel}$ ($g_{xx} = g_{yy} = g_{\perp}; g_{zz} = g_{\parallel}$).

In this case the spin-Hamiltonian is limited to the $\mathcal{H}_{\text{EZ}} = \beta_e \mathbf{S} \mathbf{g} \cdot \mathbf{B}$ term and the effective g factor can be expressed as:

$$g = [g_{\parallel}^2 \cos^2 \vartheta + g_{\perp}^2 \sin^2 \vartheta]^{1/2} \quad (2)$$

where ϑ is the angle between the applied field and the principal symmetry axis. The experimental procedure is exemplified in Figure 2 with the aid of computer simulation. For the sake of simplicity, the principal g axes of the radical are assumed to coincide with the crystal symmetry axes.

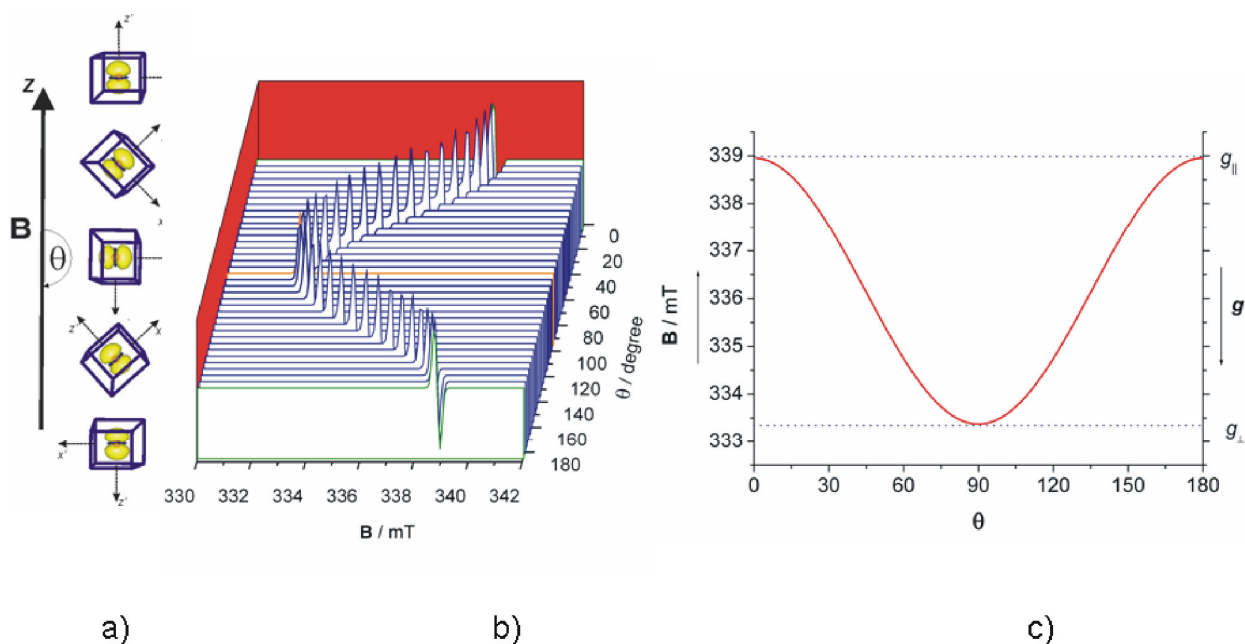


Figure 2. Angular dependence of the EPR signal of a $S=1/2$ species with axial g tensor in a single crystal. a) Orientation of the paramagnet with respect to the applied magnetic field. For the sake of simplicity the molecular axes of the radical centre are assumed to be coincident with the crystal axes. b) Computer simulation of the spectrum taken at different orientations; c) road map of the resonance signal (g and B_{res} as a function of orientation).

Single crystal EPR spectra are usually recorded with the paramagnetic crystal mounted so that it can be rotated in the resonant cavity about one of the reference axes which is normal to the applied external field. With reference to Figure 2a, by rotating the crystal in the $z'x'$ plane along the y' axis, a plot of the observed spectrum as a function of orientation of the crystal in that plane is obtained, which is shown in Figure 2b. After repeating this procedure in each of the coordinate planes, one then seeks to fit the observed curves with the theoretical formulas by adjusting the relevant parameters (in this case, g_{\perp} and g_{\parallel}) obtaining plots analogous to the one reported in Figure 2c. EPR measurements of single crystal surfaces or thin films are now available in the literature^{23,24, 25}. Although the number of EPR experiments on single crystal surfaces will probably grow in the near future, the large majority of published work refers to polycrystalline systems or powders.

3.3 Disordered systems.

Disordered systems - polycrystalline powders or amorphous frozen solutions - are composed of many small crystallites or species randomly oriented in space. To illustrate the effect of a disordered system on the EPR spectrum, let us consider the same radical in the single crystal (Figure 2) or in the corresponding powder (Figure 3). This situation is actually observed for the $O^{\cdot-}$ radical ion which was studied in KCl single crystals and at the surface of MgO powders.²⁶

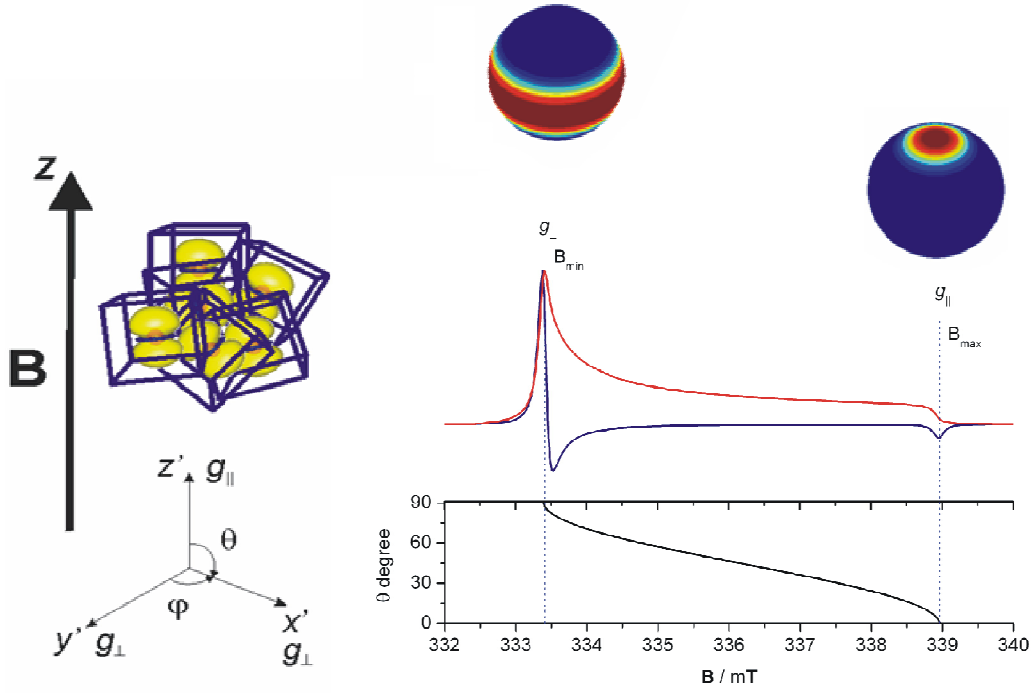


Figure 3. EPR powder pattern for the same system analyzed in Figure 2.

The resultant EPR spectrum, called a powder spectrum,²⁷ is the envelope of spectra corresponding to all possible orientations of the paramagnetic species with respect to the applied magnetic field. The simultaneous presence of resonance in the whole range between B_{\min} and B_{\max} does not create a uniform envelope, because the resonant lines are not uniformly distributed over this range.

An analytical treatment shows in fact that the microwave absorption reported as a function of the resonant field B_{res} has turning points for orientations corresponding to the principal components of the g tensor (Figure 3) which show up in the first derivative spectral trace. In other words the turning points in a powder spectrum can be individuated on the $B_{\text{res}}(\theta, \varphi)$ surface in correspondence of the points for which

$$\frac{\partial B_{\text{res}}(\vartheta, \varphi)}{\partial \vartheta} = 0 \quad (3)$$

$$\frac{\partial B_{\text{res}}(\vartheta, \varphi)}{\partial \varphi} = 0 \quad (4)$$

These equations have, in the most general case, three different solutions: $\vartheta = 0$; $\vartheta = 90^\circ$, $\varphi = 0$; $\vartheta = \varphi = 90^\circ$. Since ϑ and φ are defined in the g -matrix reference axis system, observable features correspond to orientations of the applied field along the principal axes of the g -matrix.

Referring to the simple case of Figure 3, two turning points are found in the xz plane at $\vartheta = 0$ (corresponding to g_{\parallel}) and $\vartheta = \pi/2$ (g_{\perp}). Between these two extremes a continuous absorption is observed (red line in Figure 3) the derivative leading to the typical shape of an axial powder spectrum with $g_{\perp} > g_{\parallel}$ (blue line in Figure 3). In the figure the angular dependence for the resonance is also shown (Figure 3), which indicates that in a powder spectrum, at a given value of the magnetic field only certain radicals with a given orientation with respect to the magnetic field fall “in resonance”. In other words, *specific orientations* of the radicals are successively selected by the magnetic field. With reference to the axial case of Figure 3 at the g_{\parallel} position, only one orientation, with radicals aligned along the z axis, contributes to the spectrum, as shown by the plot of orientation selections on the unit sphere. On the other extreme at the g_{\perp} position the turning point in the EPR spectrum corresponds to all the B_{res} orientations in the xy (\perp) plane. These considerations are important as by setting the magnetic field at one such turning points either single crystal-like or powder-like nuclear frequency spectra are obtained in the presence of magnetically active nuclei, by ENDOR or ESEEM techniques.^{19,28}

In real cases, CW-EPR powder spectra of surface radicals often provide challenging problems, such as heterogeneity of surface sites, presence of different paramagnetic species with overlapping signals, line broadening due to interaction between nearby paramagnetic species etc. Some of the reported complications can be overcome using advanced EPR techniques such as ENDOR or pulsed EPR. However, even in the case of classic CW-EPR, as nicely pointed out by Rieger, one frequently encounters powder spectra “sufficiently well resolved to give information rivalling that from dilute single crystal spectra”.²⁹ As it will be shown later, systematic use of tools like multifrequency EPR, isotopic substitution, computer simulation is instrumental to achieve such valuable information.¹⁶

4. Formation of radical species on solid surfaces.

Because of the difficulty of applying EPR techniques to metals, the radical chemistry is far less advanced for metal surfaces than for insulators or semiconductors. Among the latter, metal oxides, because of their dominant role in heterogeneous catalysis, either as catalysts or as supports, have been much more investigated than other compounds like sulfides, nitrides, halides etc..

The formation and stabilisation of a radical species on a solid surface have three main origins:

radical species formed by irradiation of insulating or semiconducting oxides.

In these cases an electromagnetic radiation of suitable frequency causes charge separation and formation of two distinct carriers, an electron and a positive hole. The positive hole may be

localized by an O^{2-} ion leading to a centre describable in chemical terms as an O^- radical ion, with the odd electron confined in a oxygen p orbital as shown in Figure 4a for the classic case of MgO.

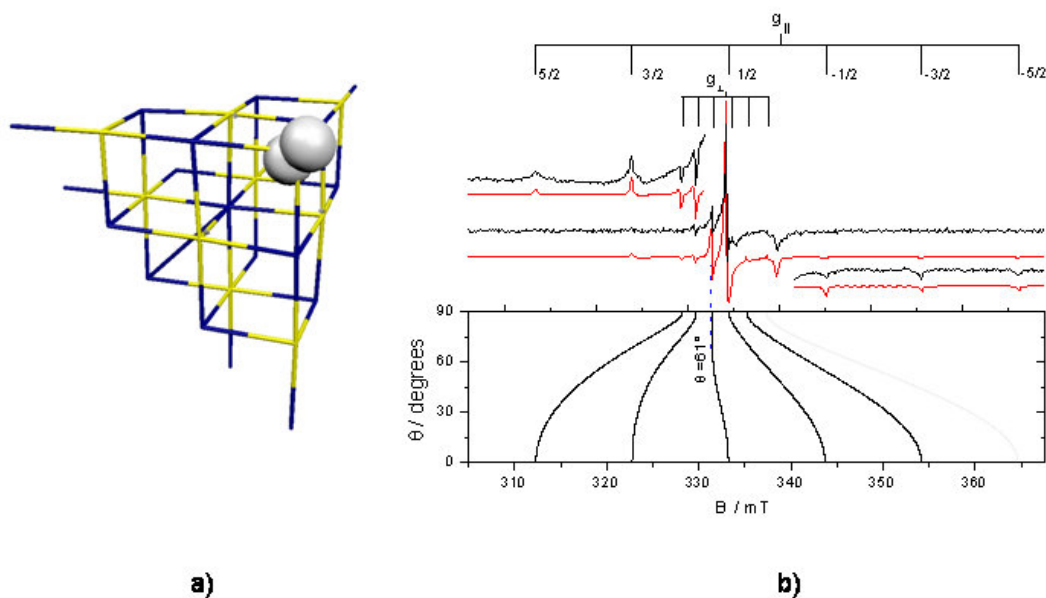


Figure 4. a) Spin density plot of an O^- ion localized at a corner site of MgO; b) corresponding experimental (77K) and simulated EPR spectra obtained for a ^{17}O enriched MgO sample. Figure adapted from ref. 26.

Its EPR spectrum obtained with ^{17}O -enriched MgO exhibits a hyperfine structure due to ^{17}O ($I = 5/2$, Figure 4b). Because the O^- radical ion is actually part of the solid, it can be seen as a surface point defect. The features of surface centres generated by irradiation will be examined in more detail in Section 4.4.

b) adsorption of a stable radical.

Important examples are nitrogen oxides (NO and NO_2) which are relatively stable molecular radicals and can be adsorbed onto surfaces. As shown later their radical character may be retained when they weakly interact with surfaces. In other circumstances they react with the surface giving rise to more complex adsorbed species (e.g. NO_2^{2-} , cf. section 8.3.2.).

c) chemical interactions at solid surfaces.

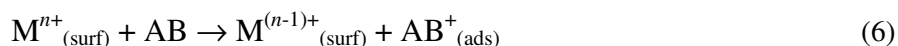
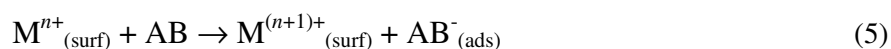
Atoms and molecules often undergo dramatic changes upon chemical interactions with solid surfaces to form either diamagnetic or paramagnetic (radical or radical ion) species. Radicals can form either upon direct interaction of a molecule with the surface or, in other cases, upon interaction between two or more molecules assisted by the surface. Chemical reactivity represents the most frequent source for the formation of surface radical intermediates. For this reason it is

convenient to schematize the basic chemical mechanisms of formation of surface radicals and to describe the types of chemical bond which are commonly formed between radicals and surfaces.

4.1. Mechanisms of radical generation at the surface.

In Section 2 we have briefly mentioned some of the basic steps in heterogeneous processes which lead to the formation of surface paramagnetic intermediates. In this Section the different mechanisms leading to the formation of a surface radical are systematically dealt with considering, for the sake of simplicity, the surface of a metal oxide containing M^{n+} cations and O^{2-} anions and a generic AB or AH molecule. The principal mechanisms leading to the formation of surface adsorbed radical species are the following:

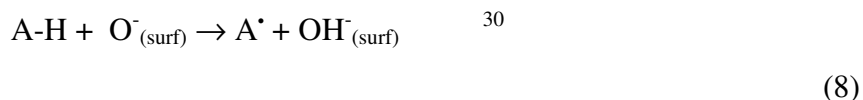
- a) non dissociative electron transfer



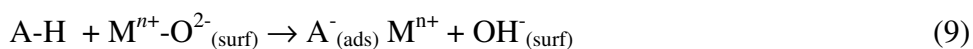
- b) surface induced homolytic splitting:



- c) atom transfer:



- d) heterolytic splitting followed by Surface Intermolecular Electron Transfer (SIET)³¹:



- e) addition or coordination of a radical AB^{\bullet} molecule



AB, in this case a radical molecule, reacts with a surface oxide ion to form a paramagnetic charged adduct (11) or coordinates onto a surface cation (12).

In the present review, we will only consider adsorbed radicals keeping in mind that, at catalytic reaction temperatures, radicals can become mobile and even desorb into the gas phase. Readers interested in the behavior of radicals in heterogeneous catalytic reactions are referred to specific papers^{32, 33}.

4.2. Chemical bonds between radicals and surfaces.

The different types of chemical bonds which exist between the surface and a radical formed by either one of the reactions given above are schematically illustrated in Figure 5 (a-d).

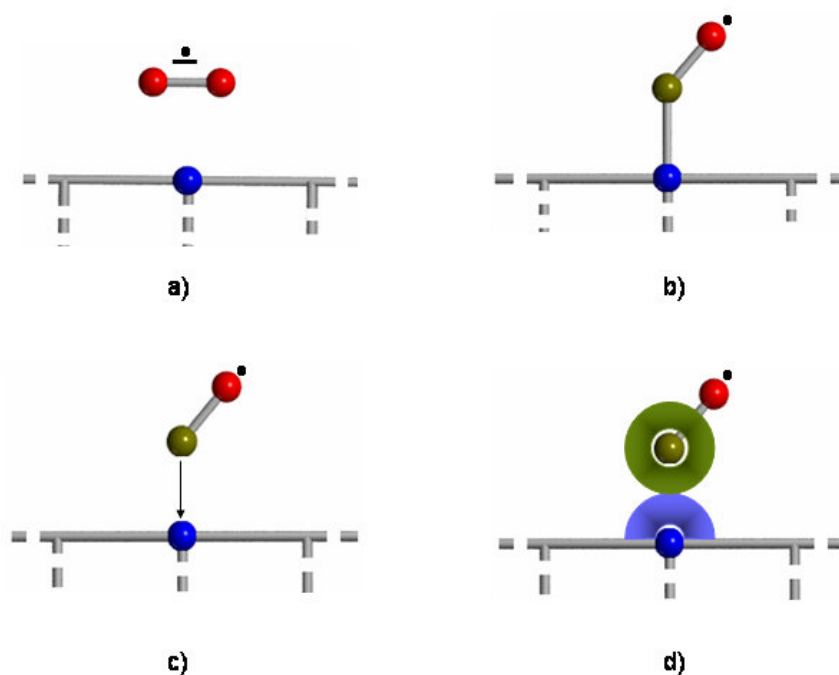


Figure 5. Possible models of chemical bonding developing between a surface and an adsorbed radical species. a) ionic bonding; b) covalent bonding; c) coordinative bonding; d) van der Waals interaction.

a) ionic bonding (Figure 5a).

Non-dissociative electron transfer (eq. 6 and 7) leads to radical ions in electrostatic interaction with the surface. This can be illustrated by the case of superoxide O_2^- ion (Figure 6) which has been widely investigated, in relation to the activation of dioxygen. Its formation at ionic surfaces can occur not only by electron transfer (equation 6) but also *via* different pathways reviewed elsewhere.³¹ The bond between O_2^- and the surface of oxides like MgO is essentially ionic, O_2^- being stabilized on top a surface Mg^{2+} cation. Analysis of the complete hyperfine structure³⁴ of adsorbed $^{17}O_2^-$ (Figure 6) leads to a spin density on O_2^- of 0.964, *i.e.*, close to unity, showing that the electron transfer from the surface to dioxygen is practically complete. The energy of ionic bonding is rather high and depends on the type of surface cation. In the case of O_2^- stabilized on low coordinated Mg^{2+} cations, values ranging between 2.5 and 3.0 eV are obtained depending on the coordination of Mg^{2+} ions.³⁵

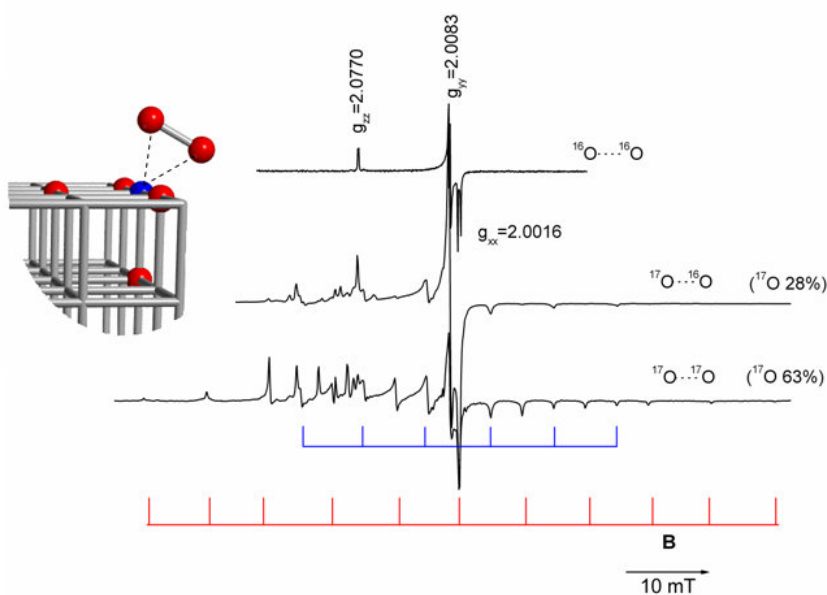
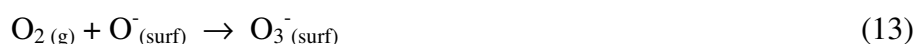


Figure 6. Schematic representation and CW-EPR spectra of the superoxide radical anion stabilized on MgO. Spectra obtained with different ^{17}O level of enrichment are shown (figure adapted from ref.34).

b) covalent bonding (Fig.5b,c)

This is the case of surface radicals formed *via* overlap of orbitals of the adsorbed species and a surface atom or ion. If the bonding involves a transition metal ion (Figure 5c) it can be described in the context of interfacial coordination chemistry.⁵ A simple example of a radical covalently bound to the surface is the O_3^- ion formed by addition of dioxygen to a surface O^- centre (eq. 14):³⁶



The ozonide radical ion is bent with a single covalent bond between the oxygen belonging to the surface and the molecule (Figure 7). At room temperature rapid rotation around this bond averages two of the rhombic \mathbf{g} tensor components.

c) Van der Waals interactions (Figure 5d)

Those are at play in physical adsorption with no electron exchange or significant orbital overlap with the surface. The physisorbed radical forms by adsorption of a molecular radical. As mentioned above the most relevant case is that of nitrogen oxides (NO , NO_2) used as spin probes of surface properties (Section 8.3).

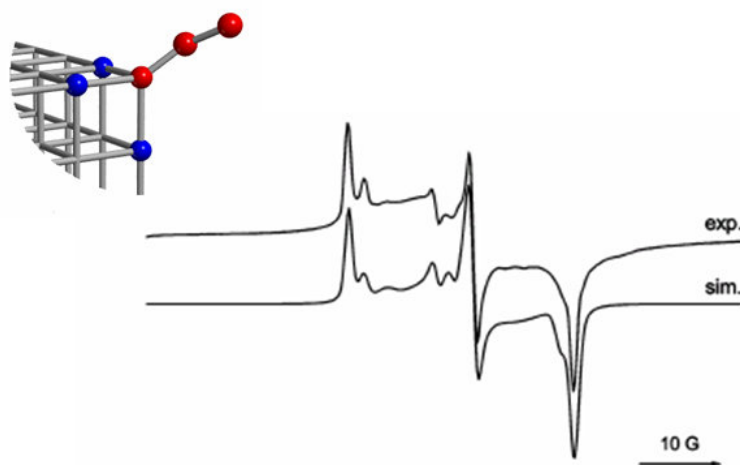


Figure 7. Schematic representation and CW-EPR spectra of the ozonide radical anion stabilized on the surface of CaO (experimental spectrum recorded at 77K). Adapted from ref. 36.

4.3 Identification and reactivity of radical intermediates in heterogeneous catalysis.

Surface science and surface chemistry investigations are necessary (though not sufficient) requirements to unravel the essential steps of catalytic reactions. The role of EPR is not limited however to preliminary characterisations of catalytic systems but can be easily extended towards the investigation of the catalytic mechanisms itself. EPR actually gave important contributions to the understanding of several catalytic processes including carbon monoxide oxidation,³⁷ dehydrogenation of ethane,³⁸ oxidation of methane to methanol and formaldehyde,³⁹ alkenes oligomerisation.⁴⁰ In two other recent cases, the role of EPR has been essential.

The first case is the oxidative coupling of methane on Li-doped MgO first investigated by Lunsford using an elegant matrix isolation approach. Methyl radicals $\cdot\text{CH}_3$ present in the gas phase over the catalyst at 773K were frozen on a sapphire rod kept in solid argon at 14K⁴¹ (Figure 8). The methyl radical, observed at low oxygen partial pressure, exhibits a quartet of hyperfine lines, with 1:3:3:1 relative intensities. The state of the surface of Li/MgO during the catalytic reaction was explored by quenching a working catalyst from the reaction temperature to that of liquid oxygen and by comparing its EPR spectrum with that of a solid slowly cooled to room temperature.

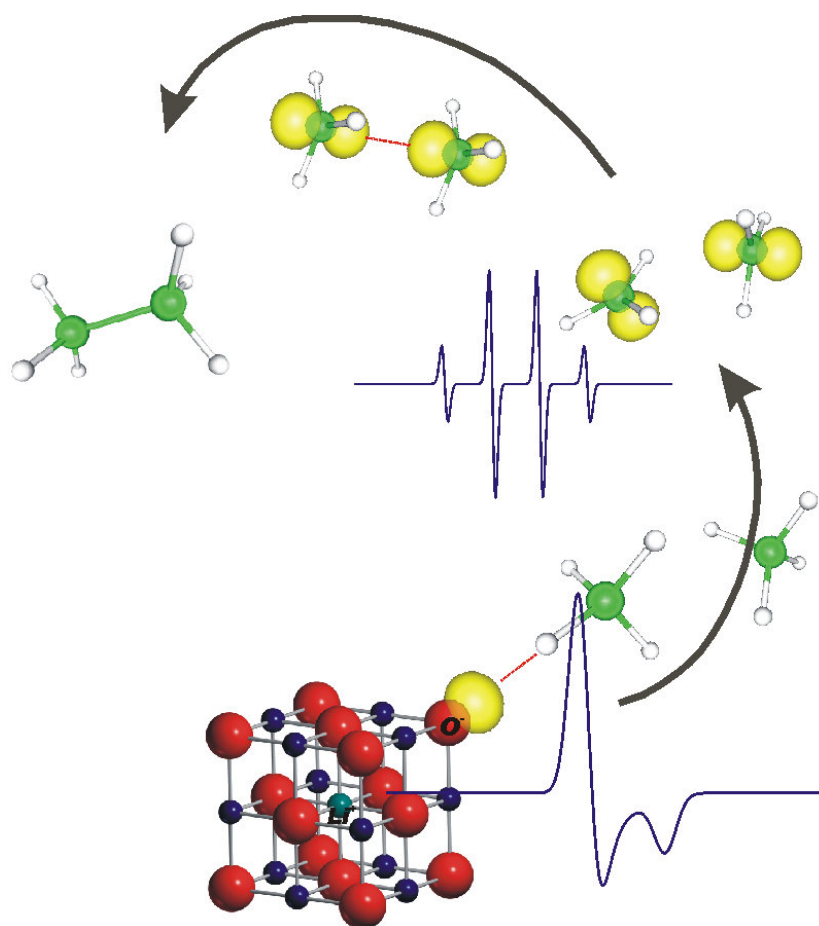


Figure 8. Schematic representation of the activation of methane on Li doped MgO. The solid contains surface exposed O^- sites which react with methane via H transfer. The O^- Singly Occupied Molecular Orbital (SOMO), in yellow, and the corresponding simulated EPR spectrum are in the bottom of the figure. Methyl radicals are formed in the gas phase (SOMO orbital, yellow, and simulated EPR spectrum in the top of the Figure) where undergo radical coupling.

In the rapidly quenched solid various paramagnetic species are present⁴² including Li^+O^- pairs (Figure 8). The O^- site (a positive hole trapped at an oxide O^{2-} ion) is able to abstract hydrogen from methane to form $\cdot CH_3$ radicals according to the heterogeneous reaction:



The formation of ethane occurs *via* $\cdot CH_3$ radical coupling while ethene forms *via* successive reactions involving ethane and again surface O^- ions, for further H abstraction. The above reaction is a true example of a heterogeneous-homogeneous catalytic reaction⁴³ i.e., initiated on the surface for the production of methyl radicals and continuing in the gas (homogeneous) phase for radical coupling. The fact that methyl radicals are neutral explains that they can easily leave the ionic surface at the reaction temperature.

The second case concerns olefins polymerisation investigated by Schmidt *et al.*^{44, 45} on a model Ziegler-Natta catalyst. Since their discovery, Ziegler-Natta catalysts have undergone a number

of improvements and modifications, which led to the so-called third generation catalysts, made of TiCl_4 supported on MgCl_2 crystals, working in presence of a co-catalyst, an alkyl aluminium compound. Despite the huge number of papers devoted to this field a detailed, atomistic, understanding of the reaction mechanism remains somewhat elusive.

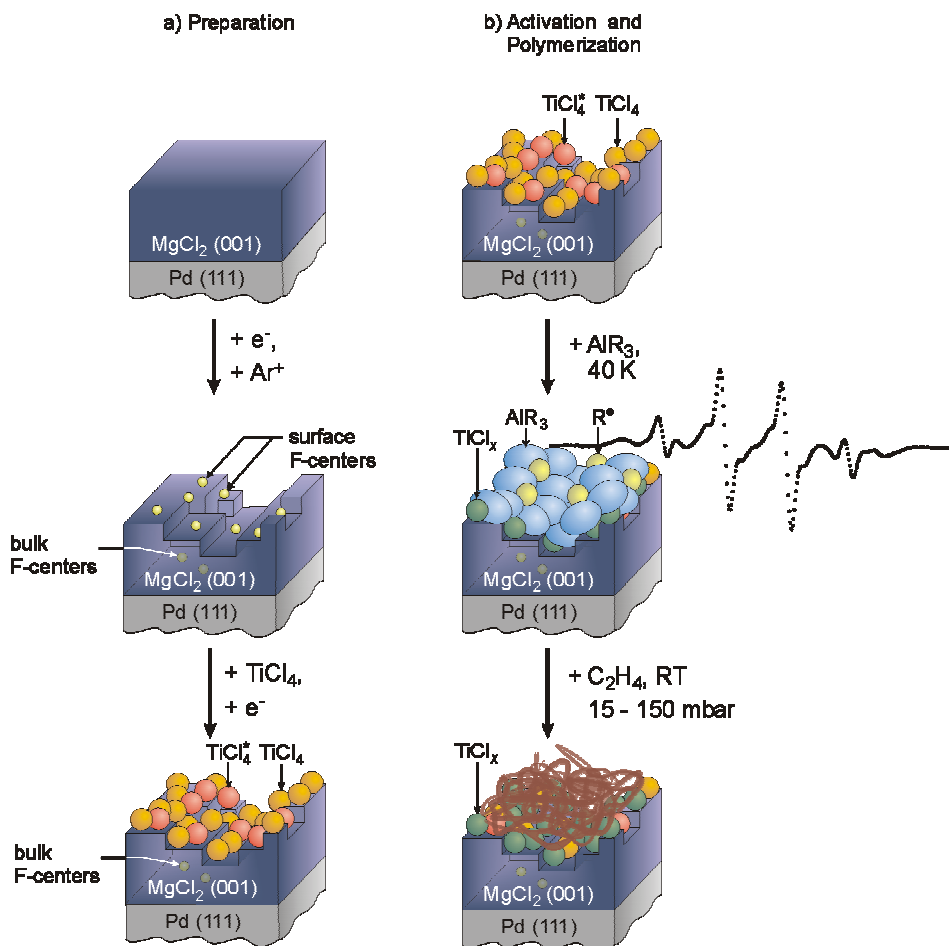


Figure 9. Preparation of the model Ziegler Natta catalyst. a) Top: preparation of a well ordered defect-free MgCl_2 film. Center: defect creation by different techniques. Color centers are symbolized by yellow spheres. Bottom: anchoring of TiCl_4 ; TiCl_4^* (red) denotes TiCl_4 moieties adsorbed to color centers. b) Top: see bottom of part a. Center: adsorption of AlR_3 on the surface at 40K; alkyl radicals are symbolized by yellow spheres. The experimental EPR spectrum recorded upon adsorption of $\text{Al}(\text{CH}_3)_3$ is also shown. Bottom: catalyst after polymerization of ethane. Adapted from ref.45

In particular, the critical process of the catalyst activation with alkyl aluminium compounds has been claimed to involve the formation of alkyl radicals. The latter have been evidenced recently by in situ EPR on a catalyst carefully prepared by means of surface science techniques (Fig.9). A MgCl_2 film was grown layer by layer on Pd(111). Defects (*F* centers) were then created in the film to favor the grafting of TiCl_4 , the active component. The EPR signal of *F* centers was observed to decrease after reaction with TiCl_4 , revealing the importance of such centers in the grafting step of the catalyst onto the support. Finally, the system is activated by exposing it to alkyl aluminium, which act as co-catalysts. Upon addition of trimethyl aluminium, the spectrum of Figure 9,

unambiguously due to ethyl radicals, was observed thus showing that alkyl radicals are indeed involved in the activation of the catalyst.

4.4 Radical intermediates in heterogeneous photocatalysis.

Photocatalysis makes use of the energy of photons to initiate a chemical process at the surface of a solid catalyst, usually a semiconducting oxide^{46,47}. Major applications of photocatalysis include the mineralization of organic pollutants, and the splitting of water into H₂ and O₂,⁴⁸ following the discovery of Fujishima and Honda in 1972⁴⁹ who observed this electrochemical photolysis at a semiconductor (TiO₂) electrode. These photochemical applications have a common starting point, which consists in the charge separation, induced by irradiation of a semiconductor (often an oxide, MO) with photons having energy higher than the semiconductor band gap. Photon absorption promotes electrons from the valence band (VB, constituted by the O²⁻ orbitals) to the conduction band (CB) leaving in the former a positive hole.



After formation the two carriers can either recombine (dissipation of photon energy) or move in the crystal. The migration of the carriers to the surface of the solid is of vital importance because chemical interactions (reduction and oxidation for the electron and hole respectively) become possible at the surface with adsorbed chemical entities. Monitoring the presence, stabilisation and reactivity of charge carriers at oxides surfaces, which often lead to EPR active species, is a crucial problem for photochemical applications of inorganic compounds and has been the object of intense EPR research, starting with the seminal work of Howe and Grätzel on colloidal TiO₂.^{50,51} Under such conditions the electron tends to localize in the *d* orbital of a cation while the positive hole moves to a nearby O²⁻ ions forming paramagnetic Ti³⁺ and O⁻ ions respectively:



Great efforts were made to improve our understanding of the state and localisation of surface stabilized carriers on TiO₂^{52,53,54,55,56} and other oxides.^{57,58} Knözinger and Diwald and coworkers, in particular, investigated the dynamics of charge separation by EPR following time-resolved responses of the photoexcited O⁻ species. They also monitored the chemical activation of small molecules like H₂ or O₂ at the surface of UV-excited nanocrystals.^{59,60} While numerous

studies dealt with the nature of the photo-generated charges, few considered the influence of the size/shape of the crystals on the electron-hole separation processes⁶¹.

Using CW and pulsed EPR techniques, Dimitrijevic *et al.*,⁶² confirmed the trapping of electrons at bulk titanium ions while the holes are trapped at surface oxygen ions. T_1 and T_2 relaxation times were measured using two pulse echo and three pulse inversion recovery techniques, which revealed that the trapped holes were interacting by weak dipolar couplings with surrounding hydrogen nuclei from adsorbed water⁶² (Figure 10). The authors also demonstrated that distortions to the Ti-O bond, resulting from reconstruction of the surface of nano-particles, caused a variation in the g -tensor values and spin lattice relaxation processes of trapped electrons. In a field largely dominated by CW EPR, this paper shows how pulsed EPR can help improve our understanding of TiO₂ surface chemistry.

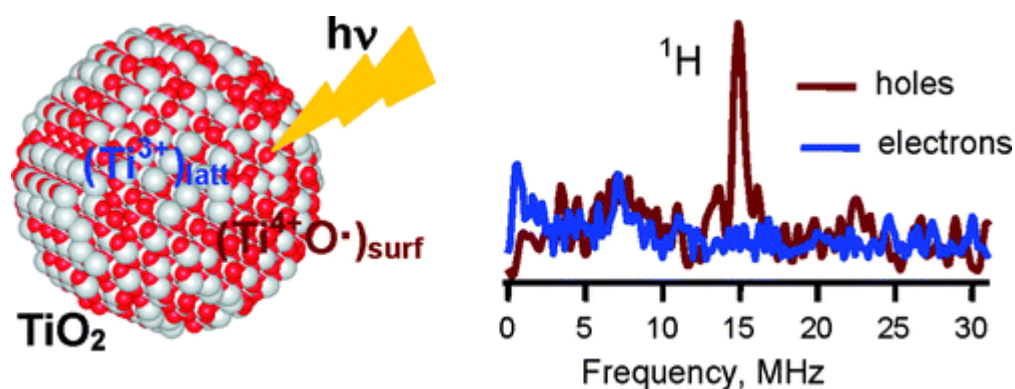


Figure 10. Typical ESEEM spectra observed upon 355 nm excitation of TiO₂ nanoparticles measured at resonant field of trapped holes (brown) and trapped electrons (blue). The peak at ¹H frequency (14.9 MHz) demonstrates that hole centres (O^{•-}) are subjected to weak dipolar coupling with surrounding ¹H nuclei from adsorbed water and are thus localized at the surface of TiO₂ particles. Reproduced from ref. 62.

Another approach to photo-catalytic investigations is to monitor surface radical species formed after reaction of a molecule with a photogenerated charge carrier. The subsequent photo-formed radical species include superoxide and ozonide ions (O₂⁻, O₃⁻) on titanium dioxide^{63, 64} or zirconium dioxide⁶⁵, CO₂⁻ from carbon dioxide on MgO and ZrO₂^{66, 67, 68}, N₂O₂⁻ from nitrous oxide on TiO₂.⁶⁹ Sections 7 and 8 will provide a systematic analysis of each type of radical.

5. Experimental approaches in EPR of surface radical species.

5.1 Paramagnetic probes of surface adsorption sites.

A problem common to surface chemistry and catalysis is to identify the adsorption sites. The same problem exists in studies dealing with surface-stabilized radicals. For such investigations,

EPR may help identify the adsorption site *via* the superhyperfine (shf) structure, based on the direct observation of the adsorbate-surface interaction (Section 3.1) and, sometimes, *via* the g tensor. The shf structure is observed only when non zero nuclear spins are present.

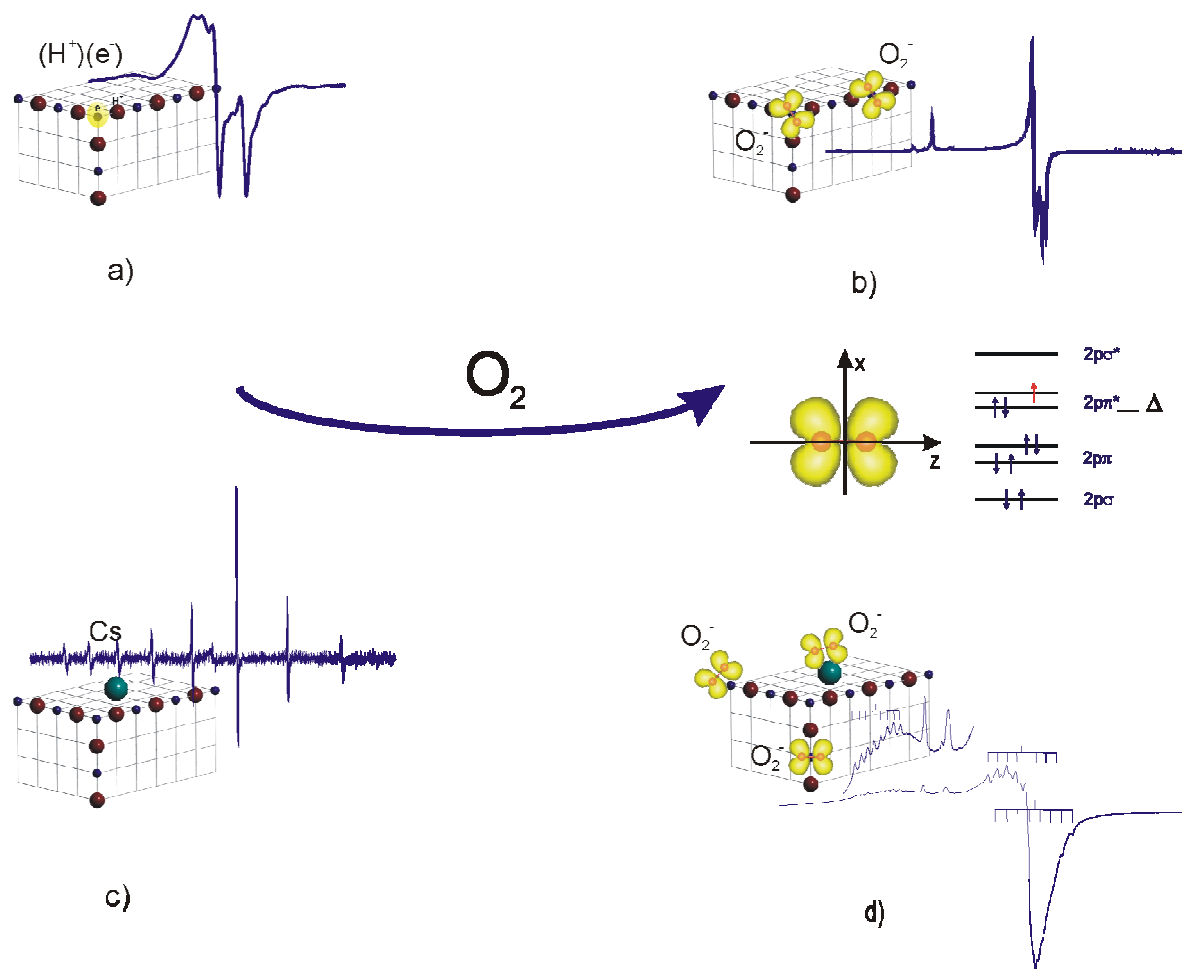


Figure 11. Surface reduction of oxygen to superoxide ion, a probe of adsorption sites. a-b) surface trapped electrons on MgO (a) and superoxide stabilisation on distinct surface Mg^{2+} sites (b). c-d) surface deposited Cs atoms on MgO (c) and superoxide stabilisation on Cs^+ and Mg^{2+} sites (d). In the central part of the Figure the SOMO orbital of O_2^- and the corresponding energy level scheme are reported.

When the shf interaction is too small, better results can be achieved using pulsed techniques. The example of superoxide O_2^- radical anions detected by CW-EPR illustrates how surface/adsorption sites can be identified (Figure 11).

O_2^- is a 13 electron π radical with three electrons in the two π^* antibonding orbitals (MO scheme of Figure 11). For ionic systems, O_2^- is usually adsorbed on a cationic site. The two limiting values of the g tensor for this species are to first order:

$$g_{xx} = g_e ; g_{zz} = g_e + 2\lambda/\Delta, \quad (18)$$

where λ is the spin-orbit coupling constant of oxygen and Δ the energy between the π^* orbitals, caused by the surface crystal field, i.e., the charge of the cation onto which O_2^- is adsorbed; z is the direction of the inter-nuclear axis and x that perpendicular to the surface. The g_{zz} component, which depends on Δ , can be used to determine, in particular in mixed oxides containing more than one type of cation, the nature of the adsorption site, because Δ is roughly related to the electric charge of the adsorbing cation⁷. The sensitivity of O_2^- to the characteristics of the adsorption goes however beyond the simple identification of the site itself. The g_{zz} component in the spectra of O_2^- ions adsorbed on binary oxides like MgO or TiO₂ is often resolved in various components monitoring distinct families of surface cations having the same nominal charge (e.g. 2+ in the case of MgO) but different coordinative environment (e.g. ions at planar faces, edges, corners).^{70, 71} Figure 11 illustrates two cases of oxygen reduction to superoxide on MgO containing electron donor centers. In one case the centers are surface trapped electrons or $(e^-)(H^+)$ centres^{72, 73} and adsorbed cesium atoms in the other⁷⁴. Figure 11 shows the EPR spectra of the starting materials. Figure 11a gives the typical signal of trapped electrons (the hyperfine doublet is due to the weak interaction of the electron with the nearby proton) and Figure 11c that of adsorbed Cs atoms with eight hyperfine lines from ^{111}Cs ($I = 7/2$)⁷⁴. Both signals disappear upon interaction with oxygen and new signals due to O_2^- appear. The first one (Figure 11b) is characterized by three g_{zz} values (2.091, 2.077, 2.065) corresponding to three distinct Mg^{2+} ions. No superhyperfine structure due to ^{25}Mg ($I = 5/2$) is observed, probably because of its low natural abundance (10%). The site discrimination is based, in this case, on the g tensor only.⁷⁰ The second O_2^- spectrum (Figure 11d) is more complex with a eight-line shf structure due to ^{111}Cs associated to the three g components. Additionally, two unstructured lines at $g = 2.077$ and $g = 2.065$ correspond to O_2^- adsorbed on Mg^{2+} . This indicates that superoxide ions are formed by electron transfer at the expenses of Cs atoms and that a fraction of the radical ions is stabilized on the resulting Cs^+ cations while a second fraction undergoes spill over towards the matrix sites.

In summary, EPR can provide not only information on the nature (e.g. O_2^-) and structure (e.g. side-on) of the adsorbed species but also on the nature (e.g. Cs^+) and structure (e.g. Mg^{2+} at corners, edges, faces) of the sites present at the surface.

5.2 Molecular motion of adsorbates on solid surfaces.

As mentioned in Section 3, EPR can help investigate the dynamics of paramagnetic adsorbates, which is of major interest in surface science and catalysis. The time scale typical of

most spectroscopies, in particular electron spectroscopic methods, is too short to detect molecular motions, which are in the range 10^{-6} - 10^{-10} s. This is the operating regime of EPR (Table 1) which is thus very useful to study molecular dynamics at the gas-solid interface.

The EPR spectrum dramatically depends on the rate of the tumbling which results in a loss of the spin density anisotropy. Two motional regimes can be distinguished; 1) fast regime, where the correlation time is much smaller than the microwave frequency, which results in a complete loss of spectral anisotropy leading to line narrowing); 2) slow regime,⁷⁵ where the interactions of the unpaired spins, determining the shape of the EPR spectrum are modulated through molecular dynamics giving rise to distinct EPR spectral features, which enable to distinguish among different forms of molecular motion and adsorbate orientations. This regime is particularly informative on local structure and dynamics of adsorbates.

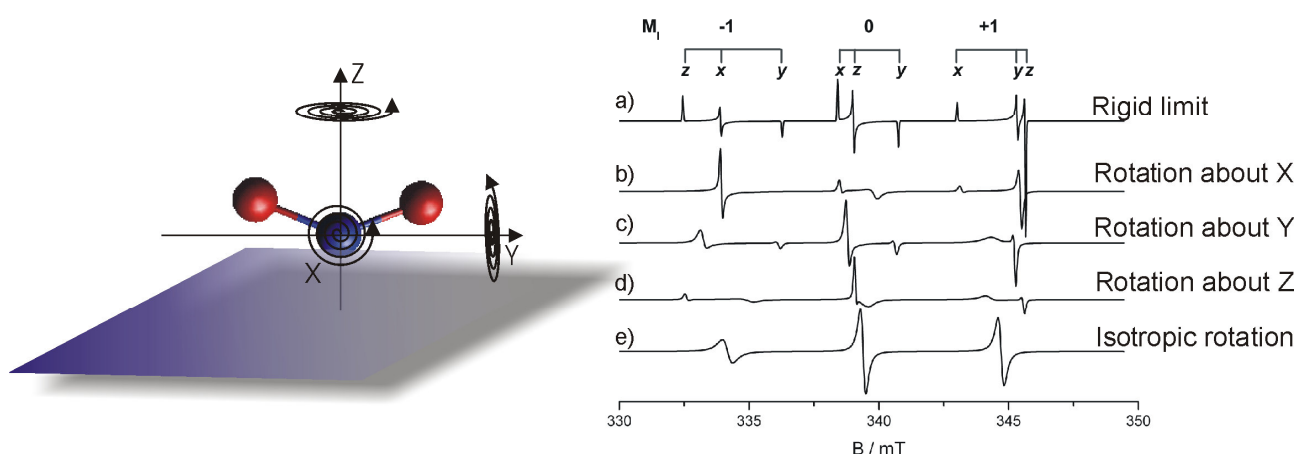


Figure 12. Theoretical spectra illustrating the change of the EPR spectrum of NO_2 occurring as a function of rotation about different molecular axes. a) rigid limit, b) rotation about the X axis, c) rotation about the Y axis, d) rotation about the Z axis; e) isotropic rotation. The rotational correlation time about a given axis was set to 1×10^{-8} s, while rotation about the perpendicular axis was 5×10^{-5} s.

EPR has been employed to investigate the local dynamics of NO in different molecular sieves,⁷⁶ as well as O_2 on different surfaces.⁷⁷ The adsorption of NO_2 on copper,⁷⁸ Vycor glass,⁷⁹ silica gel⁸⁰ and a number of other matrixes has been studied in details. EPR studies are also available on NO_2 in rare gas matrixes^{81,82,83} and $\text{NO}_2/\text{N}_2\text{O}_4$ thick films⁸⁴, where preferential orientations were obtained by deposition of the gases on flat surfaces. Importantly, EPR investigations of NO_2 on single crystal surfaces of clean Au (111)⁸⁵ and Al_2O_3 (111)⁸⁶ under UHV

conditions have also been reported, which give insights into the geometrical arrangement and local dynamics of the adsorbate.

To exemplify the potential of EPR in studying the orientation and dynamics of adsorbates on surfaces in the following we will illustrate the case of NO₂, which can be considered as an effective surface “spin probe” and for which detailed data are available on powders and single crystal surfaces. We discuss here the results reported by Shiotani and Freed⁷⁹ on NO₂ adsorbed on Vycor glass (Table 4). In Figure 12a the computer simulation for the rigid limit (the adsorbed molecule is immobile) is reported and the different components (x, y and z) for the three M_I quantum numbers are shown. The features of the spectrum are due to two main contributions. The first is the electron Zeeman interaction, giving an anisotropic g tensor ($g_x \neq g_y \neq g_z$) whose components correspond to three distinct resonant fields. Each g component is then split into three lines due to the hyperfine interaction of the unpaired electron with the nuclear spin of N ($I=1$).

The EPR spectra shown in Figure 12 b-e following the work by Shiotani and Freed,⁷⁹ correspond to the effect of rotation of NO₂ about the molecular axes X, Y and Z indicated. The simulation was performed using the Easyspin package⁸⁷ imposing a diffusion rate about a given axis of $1 \times 10^8 \text{ s}^{-1}$ while a value of $5 \times 10^5 \text{ s}^{-1}$ was used for the perpendicular axis. In this way the A and g tensor components perpendicular to the rotational axis are averaged out, while the other components are only slightly broadened. For example for rotation about the X axis (Figure 12b) it can be seen that the x components remain at their rigid limit position and are only slightly broadened while the y and z components are averaged out. The same arguments apply to the other cases clearly showing how information on motion can be revealed by the spectrum. Finally in Figure 12e the case of isotropic motional averaging is shown, which leads to the collapse of all anisotropies, which are reflected by the line width dependency on M_I. Analysis of the experimental spectra in the range 4.2-220 K led Shiotani and Freed⁷⁹ to conclude that the NO₂ molecule adsorbed on Vycor glass undergoes rotation about the Y axis (suggested to be parallel to the surface) at temperatures below 77K, while an isotropic motion likely due to translational diffusion is observed at T>77K.

The EPR spectra of NO₂ at coverages below the monolayer on an oxide single crystal under UHV conditions have been reported by Schlien *et al.*⁸⁶ These studies are particularly interesting as they allow in principle to establish the orientation of the molecular radical on the surface, i.e. what is the molecular axis about which the motion occurs. In the case of NO₂ on the 111 surface of Al₂O₃ no rotational motion was found below 100 K, indicating that the rotational correlation time is longer than 10^{-7} s. The EPR spectra were found to be drastically influenced by translational diffusion of the

NO₂ monomers on the surface, which lead to dimerization ($2\text{NO}_2 \leftrightarrow \text{N}_2\text{O}_4$) and loss of the EPR spectrum.

6. Main families of surface inorganic radicals: electronic configurations and geometry.

For the sake of clarity surface radical species can be classified as it is done in gas phase or in various matrices². It is however convenient, first, to introduce their most common structural and electronic features. In some cases, it happens that radicals and radical ions observed at surfaces have their bulk analogs (in rare gas matrices or in solids) often with a different structure (section 4.2). Other radicals have never been isolated in a matrix and are typical of surfaces.

The influence on EPR parameters of the electronic configuration and the nature of the SOMO have been discussed by Atkins and Symons¹ for inorganic radicals on the basis of Walsh diagrams. These diagrams, giving the energy of molecular orbitals as a function of bond angles, are based on the rules formulated by Walsh⁸⁸ which relate the shape of a molecule in a given structural class to the number of valence electrons. The most important rule states that a molecule adopts the structure that best stabilizes its *highest occupied molecular orbital* (HOMO). If the HOMO is unperturbed by the structural change under consideration, the occupied MO lying closest to it determines the preferred geometry. The first principles foundations for these empirical rules have been clarified by March.⁸⁹ In the following we will refer to this systematic classification. In some cases, the structural features and the SOMO orbitals calculated for the gas phase radicals using the GAUSSIAN 03 code will also be reported⁹⁰.

6.1 Monoatomic species.

Among single metal atoms, the most widely investigated in EPR are those having a $^2S_{1/2}$ non degenerate electronic state because they give rise to spectra easily observable. This is the case of hydrogen and alkaline metals whose spectra are characterized by an hyperfine structure because of their non zero nuclear spin.

Hydrogen atoms trapped in the bulk of different matrices exhibit spectra characterized by large hf coupling constants rather close to the gas-phase value.¹³ A remarkably different situation is found when H atoms are stabilized by the surface of ionic oxides. Hydrogen atoms spontaneously dissociate on the surface of alkaline-earth metal oxides to give blue colored samples which exhibit intense and complex EPR spectra. The nature of these surface paramagnetic species, which has been recently elucidated by some of us,⁹¹ can be described in terms of unusual (the simplest) (H⁺)(e⁻) ion pairs stabilized on low coordinated sites of the ionic surface (Figure 11a). It should be pointed out

that this unusual hydrogen chemistry, only observed on insulating ionic oxides, is due to the strong proton affinity of the very basic O^{2-} surface ions coupled with the energy gain obtained by trapping the electron near low-coordinated M^{2+} cations.

Alkali metal atoms have been studied in a variety of solid matrices,⁹² liquid solvents² and, only recently, at surfaces.⁹³ In all cases the matrix influences the electronic properties of the metal atom (matrix effect) as reflected by the hyperfine coupling constant of the EPR spectra.⁹⁴ Typically, the EPR spectra of trapped alkali atoms in frozen rare gases and hydrocarbons exhibit hyperfine interactions which depart by only a few percents from the gas phase values.⁹²

A drastically different situation occurs when alkali metal atoms are deposited on basic oxides such as alkaline-earth oxides.^{93,95} A consistent reduction (about 50%) of the hf coupling constant with respect to the gas phase value is observed in this case, which implies a strong perturbation of the unpaired electron wave function. A very similar effect is observed when alkali metals are dissolved in solvents such as methylamines or crown ethers,^{96,97} the common feature with alkaline-earth oxides being the ability of the matrix to donate a lone pair. Upon interaction with the lone pair localized on a surface O^{2-} ion, the ns orbital of the alkali atom containing the unpaired electron is destabilized, leading to an “expanded” atom structure reminiscent of a Rydberg state.⁹³ This intriguing situation, which seems to be a general feature of alkali metal atoms interacting with basic solvents, is fully supported by theoretical calculations,^{93,98} which allow to rationalize the matrix effect within the framework of Pauli repulsions.

The same arguments were adopted by Yulikov *et al.*⁹⁹ to explain the reduction of the Au hf coupling constant observed when Au atoms are deposited on a MgO thin film (Figure 13).

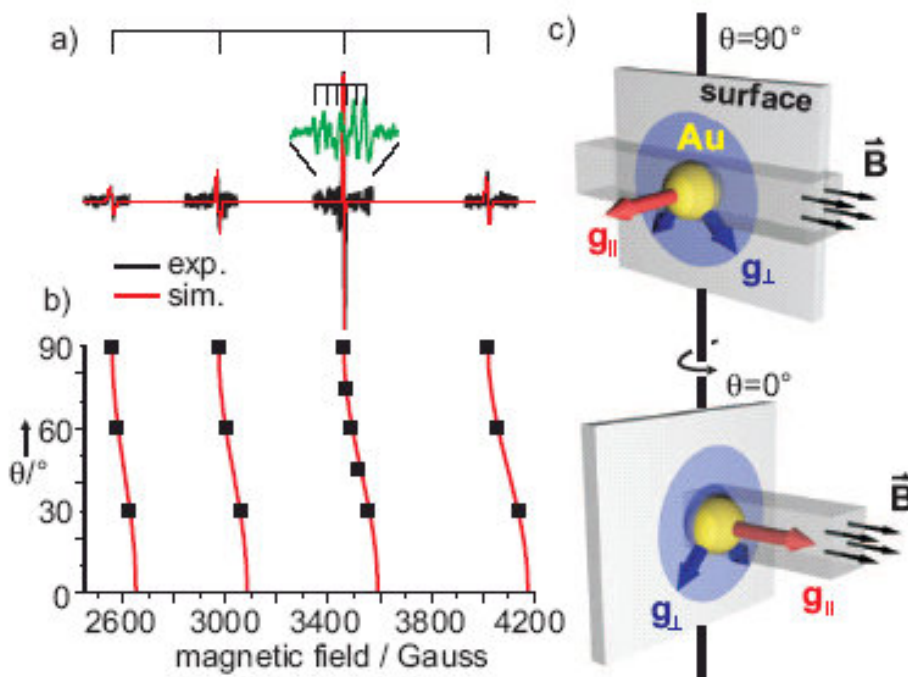


Figure 13. Experimental and simulated EPR spectrum of Au atoms adsorbed on MgO(001)/Mo(100). The angular dependance of the reonance position and the orientation of the g components with respect to the applied magnetic field are also shown. Figure reproduced with permission from ref. 99.

It is interesting to compare these results with those obtained by Mile and co-workers¹⁰⁰ when depositing coinage metals (Cu, Ag, Au) on alkali metal chlorides by means of the rotating-cryostat technique. Although this technique leads typically to bulk-like species, in this particular case the authors suggest that the metal atoms may be trapped at asymmetric sites located at the interface between layers of the alkali metal chloride, resembling species trapped at surfaces or grain boundaries rather than in the bulk. Indeed the EPR spectra show much lower hyperfine interactions than for atoms prepared in alkali-metal chloride single crystals from metal ions in cationic substitutional sites by electron capture^{101,102} and are in line with the spectra reported by Yulikov *et al.*⁹⁹ for Au deposited on MgO. Finally it is interesting to note that the trend observed by Mile and coworkers.¹⁰⁰ for coinage metals on alkali-metal chlorides (LiCl, NaCl, KCl) parallels the trend reported by some of us^{93,103} on alkali metals deposited on alkaline-earth oxide (MgO, CaO, SrO). In both cases a nearly linear relation can be found between the metal hpf coupling constant and the lattice parameter. This trend has been discussed earlier¹⁰³ in terms of increasing lone pair donaticity (i.e. Lewis basicity) brought about by the reduced Madelung potential around the basic O^{2-} ion as the lattice parameter increases.

Systems having orbitally degenerated ground state are hardly observed in EPR in a inert matrix. Their orbital angular momentum however is sensitive to asymmetric environments so that

they can be observed, as “quenched” species, in crystals or at surfaces, the field acting at the surface being by often asymmetric. This fact, which will be widely discussed in the following for diatomic molecules and radical ions, is also true for some monoatomic species like O^- (Figure 4) and S^- which have been identified in a number of cases.

6.2. Diatomic radical species.

While $^2\Sigma$ systems prevail in the field of matrix isolation, the most important biatomic surface radical species are $^2\Pi$ radicals. Hardly observed in an inert matrix, because their spectrum, spreading over a large domain of magnetic field, becomes undetectably weak, $^2\Pi$ radicals have been, in some case, individuated in ionic matrix whose electric fields can more efficiently perturb the degenerate orbital states. In this case they are referred to as quenched species. The asymmetric field typical of a surface is also a powerful quenching agent so that EPR spectra of surface adsorbed $^2\Pi$ are easily observed. Examples of both possible substates of a $^2\Pi$ molecule ($^2\Pi_{1/2}$ and the $^2\Pi_{3/2}$) have been observed. Eleven electron radicals like NO, N_2^- , CO^- have one electron in 2π antibonding orbitals and $^2\Pi_{1/2}$ ground state, while thirteen electrons radicals like O_2^- or ClO^- have three electrons (or one positive hole) in these orbitals and $^2\Pi_{3/2}$ ground state (Figure 14).

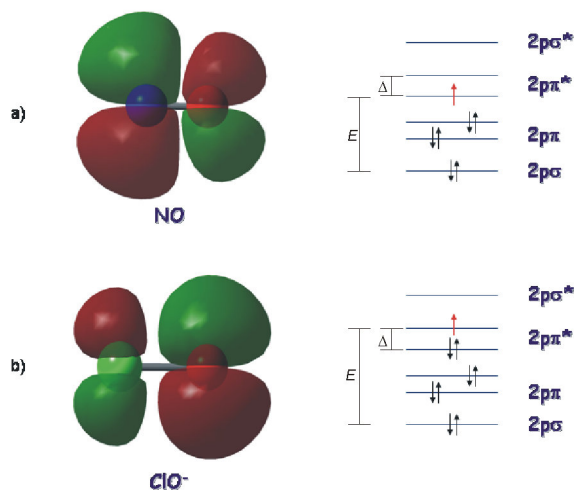


Figure 14. SOMO orbitals of representative $11e^-$ (NO) and $13e^-$ (ClO^-) radicals in gas phase. The energy level schemes in the right hand side are referred to the same species in the adsorbed state.

The diatomic radicals mentioned above are often crucial intermediates in the activation of small molecules. Some of them are important also to probe surface crystal fields and to identify adsorption sites (Sections 5, Figure 11). Nitric oxide (NO) and the superoxide radical ion (O_2^-) are the two most widely used probes.

6.3 Triatomic, tetra-atomic and penta-atomic radical species

A variety of polyatomic radical and radical ions have been observed at surfaces. All of them have non degenerate ground state with well separated energy levels so that they are insensitive to the influence of local crystal fields. The observed g tensors are close to those observed for their matrix isolated analogs (if any) and can be considered fingerprints of the species. We will describe in the following two families of triatomic surface radical species both having non linear structure.

The former family includes radicals with 17 valence electrons like CO_2^- and NO_2 . The electronic structure of these species can be easily understood starting from that of the linear, 16 electrons CO_2 molecule. The 17th electron cause the molecule to bend and the SOMO (2A_1 symmetry) has the features of a π antibonding orbital built up by three parallel p orbitals on C and O atoms with a contribution of the carbon 2s orbital¹ (Figure 15).

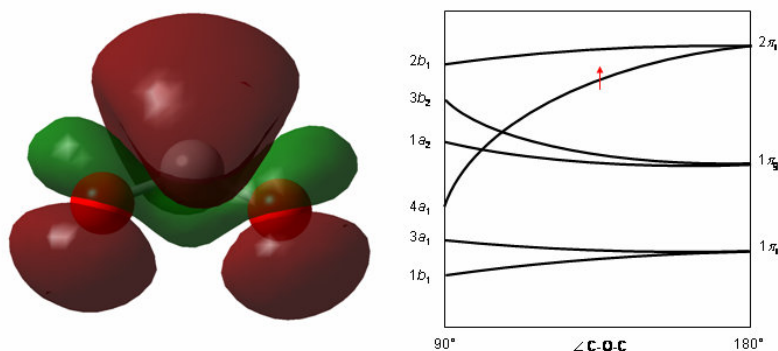


Figure 15. SOMO orbitals and Walsh diagram of the molecular orbital energy of the CO_2^- radical ion in gas phase

This involves a considerable isotropic splitting in the EPR spectrum from the central atom (${}^{13}\text{C}$ and ${}^{14}\text{N}$ or ${}^{15}\text{N}$ in the examples proposed) which adds to the anisotropic one, typical of p orbitals.

By contrast, for bent 19 electrons species (O_3^- , NO_2^{2-} , ClO_2) the isotropic coupling is instead not expected (except for a small contribution due to spin polarization) because the odd electron is now in the orbital which is formed purely by antibonding interaction of the other three parallel π orbitals on the three atoms (2B_1 symmetry, Figure 16a).

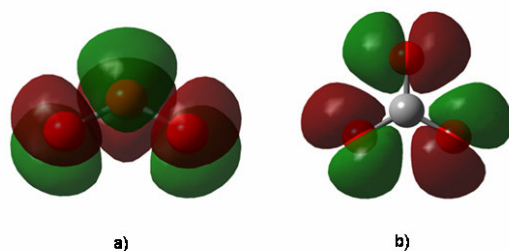


Figure 16 SOMO orbitals of O_3^- (a) and CO_3^- (b) radical ions in gas phase.

Among the tetra-atomic radical species we will consider cases of 21, 23 and 25 valence electron respectively, the latter two having matrix isolated analogs.

Twenty three electrons radicals like CO_3^- or NO_3^- generally have planar D_{3h} symmetry. The SOMO, built up by the out of phase combination of in plane p orbitals of the outer atoms (oxygen in our case), is essentially non bonding (2A_2 symmetry) so that no or very small contribution from the central atom to the hyperfine structure is expected and these species can be actually defined as tetra atomic planar σ radicals (Figure 16b).

25 electron radicals like NO_3^{2-} and ClO_3 generally have pyramidal C_{3v} symmetry. The electronic structure recalls that of 17 electron radicals because the 25th unpaired electron upon entering the antibonding $2a_2$ orbital causes bending of the 24 electron planar structure. The distortion introduces some s character (from the s orbital of the central atom) to this orbital reducing its antibonding character. The SOMO has thus a 2A_1 symmetry and both isotropic and anisotropic hpf contributions from the central atom are expected.

The twenty nine electrons radicals observed at surfaces are low symmetry molecules without analogs among matrix isolated species so that no detailed analysis of the electronic structure comes from previous studies.

7. Carbon containing inorganic radicals.

The interest of this family of surface radicals comes from the importance of the chemistry of carbon oxides. The activation of carbon oxides may be achieved *via* heterogeneous catalysis, by surface photochemistry and also *via* mechano-chemistry. While the catalytic conversion of CO has always been a basic topic in heterogeneous catalysis, the interest in the artificial conversion of CO_2 is more recently triggered by its impact on global warming and sustainability¹⁰⁴. CO_2 is

thermodynamically very stable and its conversion requires high free energy chemicals or an external supply of thermal, electrical or photochemical energy. Radicals are often intermediates of surface chemical processes involving carbon oxides. The relevant members of the family are illustrated in the following.

7.1 The CO_2^- radical anion.

The CO_2^- carboxylate radical anion was first observed by Lunsford and Jayne¹⁰⁵ upon adsorption of CO_2 on UV-irradiated MgO containing trapped electrons, following the direct electron transfer reaction:



The same radical, with slightly different EPR parameters, was also observed^{106,107} after adsorption of CO on MgO containing O^- ions, following the reaction:



A detailed X- and Q-band EPR study of the CO_2^- radical using ^{13}C and ^{17}O labelling was undertaken by Vedrine and co-workers¹⁰⁸ on irradiated MgO. The formation of the carboxylate radical anion on “electron rich” MgO was recently revisited by some of us in the light of the advanced understanding of excess electron centres on the surface of alkaline-earth oxides^{109,110}. The results confirm those reported earlier¹⁰⁵ leading to a detailed mapping of the unpaired electron spin density distribution over the entire radical anion. The EPR spectrum of CO_2^- displays rhombic g tensor ($g_1=2.0026$, $g_2=2.0009$, $g_3=1.9965$) very close to that observed for its analogs irradiated carbonates.¹¹¹ CO_2^- is a 17 electrons radical with its unpaired electron in the first π_u^* orbital of the CO_2 molecule, built from three parallel p atomic orbitals. The extra electron causes the molecule to bend thus introducing a partial admixture of the $2s$ carbon orbital to the SOMO orbital (Figure 17). This fact explains the structure of the nearly axial ^{13}C hyperfine tensor ($I(^{13}\text{C}) = 1/2$) with $A_1= 181$ G, $A_2= 224$ G and $A_3 = 177$ G (Table 3), in good agreement with the parameters of the same species observed in irradiated sodium formate.¹¹¹ As discussed in Section 4, the non degenerate ground state makes the radical rather insensitive to the local crystal field, explaining the similarity between the parameters of the radical on the surface or in the bulk of irradiated crystals.

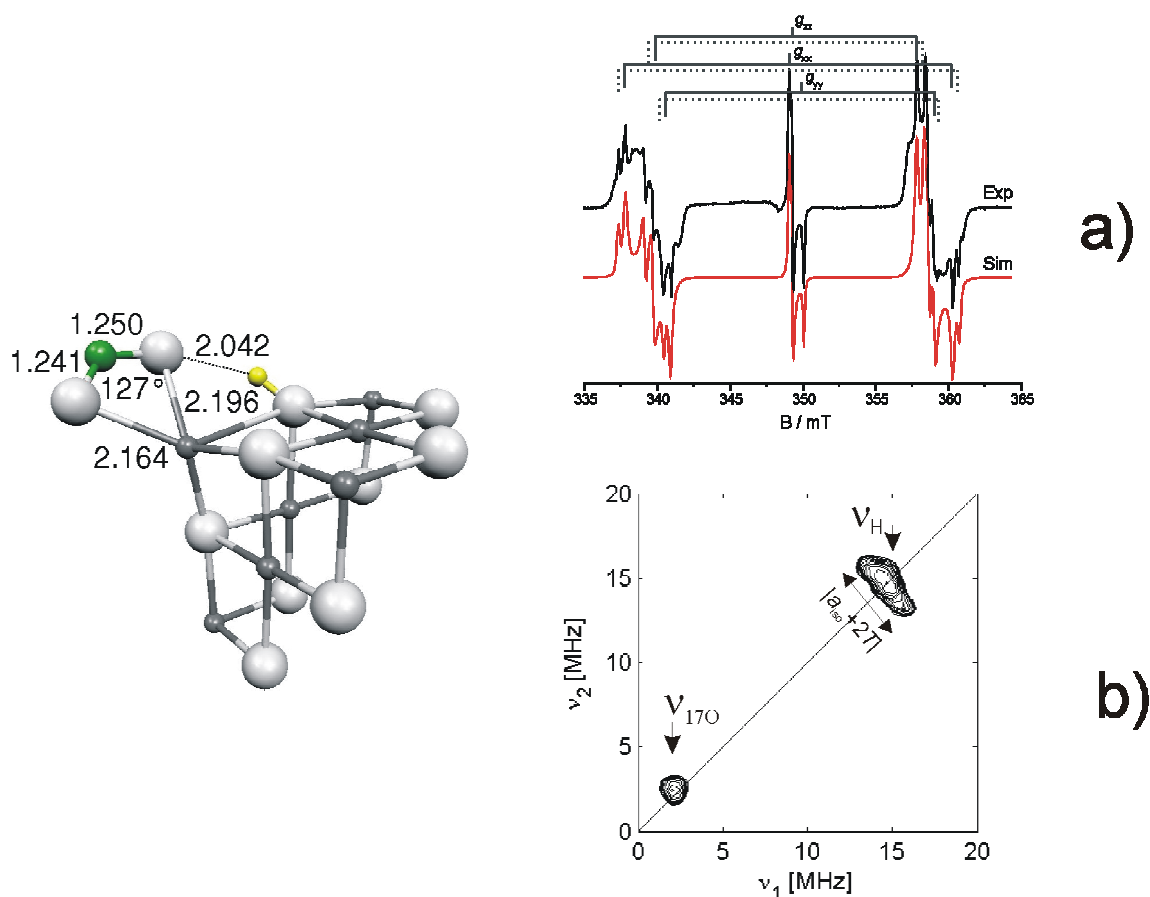


Figure 17. Calculated structure and EPR spectra at 77K of the CO_2^- radical ion stabilized on MgO obtained by CO_2 adsorption on the surface containing trapped electrons. a) CW EPR spectrum of ^{13}C enriched CO_2^- ; b) Hyperfine Sublevel Correlation Spectroscopy (HYSCORE) spectrum of the same radical stabilized on a ^{17}O enriched MgO matrix. Adapted from ref.110.

The ^{13}C hyperfine structure indicates a spin density mainly associated to the $2p_z$ carbon orbital (z being the direction perpendicular to the molecular plane) with $c^2(2p_z) = 0.45$ and $c^2(2s) = 0.18$. ^{17}O labelled CO_2 allows to determine the ^{17}O ($I = 5/2$) nearly axial hyperfine tensor of CO_2^- adsorbed on MgO:¹⁰⁹ $A_1 = 24$ G, $A_2 = 60$ G and $A_3 = 25$ G, in agreement with earlier work on the same system¹⁰⁸ and with results on bulk radicals in irradiated sodium formate.¹¹² The O nuclei are found to be equivalent, suggesting a side-on structure on low coordinated Mg^{2+} cations which is shown in Figure 17 together with the CW-EPR spectrum of the ^{13}C enriched radical.¹⁰⁹ As a complement to CW results, pulse-EPR experiments allowed the observation of the coupling of the carboxylate radical with a nearby proton belonging to a surface OH^- group resulting in the following superhyperfine tensor $A(\text{H}) = [-3.5 \ -4.3 \ +3.9]$ MHz. These results, together with DFT calculations enabled to establish the location and geometry of the adsorbed CO_2^- radical anion (Figure 17)¹¹⁰.

Quite recently it has been shown that photoreduction of CO₂ to CO takes place on MgO under UV irradiation in the presence of hydrogen or methane as reducing agents⁶⁶. The process starts with the photoinduced formation of a CO₂⁻ radical ion whose spectrum is similar to those described before. The radical ion is reduced in the dark to form a formate or an acetate by hydrogen and methane respectively. A very similar mechanism was proposed by the same authors for the photoreduction of CO₂ to CO on ZrO₂ (zirconia). The photoformed CO₂⁻ radical, observed for the first time on ZrO₂, reacts with hydrogen in the dark^{66,67,68} during the successive steps of the reaction.

The formation of CO₂⁻ was also observed on silica gel, UV-irradiated under an atmosphere of O₂ and CO¹¹³. The authors suggested that a photogenerated hole centre of O⁻ reacts with CO to form CO₂⁻ with the scheme reported in eq.20.

7.2 Radicals generated from carbon monoxide.

While CO₂ does not form paramagnetic species by reaction with the surface of bare MgO, carbon monoxide leads to a complex chemistry which involves both radical and diamagnetic species. The first observation of a paramagnetic species by adsorption of CO on thermally activated MgO was reported by Lunsford and Jayne¹¹⁴. The axial spectrum ($g_{\perp}=2.0055$ and $g_{\parallel}=2.0021$) was assigned to a surface bonded monomeric carbonyl species. The formation of the radicals is very slow and the EPR spectrum takes weeks to reach its maximum intensity. A similar spectrum, observed later by Klabunde on MgO¹¹⁵ and Cordischi et al on Co²⁺/MgO¹¹⁶, was independently assigned to the dimer C₂O₂⁻ radical anion. This assignment was based on ¹³C labelling experiments and computer simulation showing two equivalent carbon atoms. It is not surprising that Lunsford and Jayne¹¹⁴ were unable to draw the same conclusion because their experiment with ¹³CO was affected by the presence of a large percentage of ¹²CO, leading to spectral features obscuring the central line of the ¹³CO signal. Further work, also by Klabunde's¹¹⁷ and Cordischi's¹¹⁸ groups, questioned the earlier hypothesis of the dimer radical ion proposing that the radical was in fact C₆O₆³⁻ adsorbed with only two carbons interacting with the unpaired electron. The work was extended by Morris and Klabunde¹¹⁷ to CaO, leading to spectra very similar to those recorded with MgO and to the same assignment.

The chemistry of paramagnetic CO species was revisited in the 1990's by Giamello *et al.*¹¹⁹ who investigated two different surfaces of MgO: one bare and the other, called electron-rich, obtained by ionisation of alkali metals on MgO and containing surface-trapped electrons. Upon interaction with CO the latter surface gives an EPR signal which is the same as the one slowly developing on thermally activated bare MgO. Spectra obtained using ¹³CO confirmed the presence

of two magnetically equivalent carbon atoms in the species. On the basis of both theoretical calculations¹²⁰ and low temperature experiments¹¹⁹ it was proposed to reassign the EPR spectra to the dimeric $C_2O_2^-$ ethyldione radical ion originally proposed by Klabunde's¹¹⁵ and Cordischi's¹¹⁶ groups.

Contacting the electron rich solid with CO at 77K and carefully rising the temperature the early steps of CO reduction were followed. Using ^{13}C - and ^{17}O -enriched CO, it was possible to assign the spectra obtained at 100K to the monomer radical anion CO^- and to evaluate the spin density distribution on this previously unreported species. The g tensor measured on the simpler ^{12}CO spectrum showed two components to be close to the free spin value and a third one at $g \cong 1.98$ which is the unambiguous fingerprint (Section 6.2) of a 11-electrons π radical, like NO.

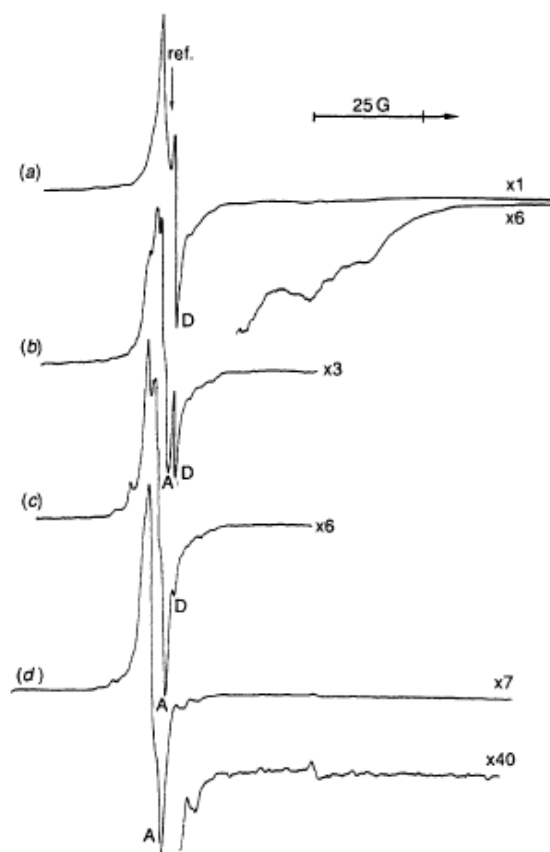
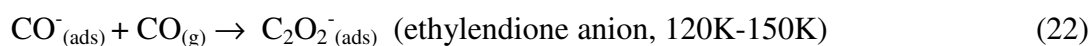
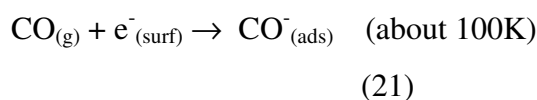


Figure 18. EPR spectra observed after adsorption of CO at 78K on surface electron rich MgO and heating at increasing temperature. Spectrum a) was observed after heating at about 100K and is due to the CO^- radical anion. All spectra were recorded, after temperature increase, at 77K. Figure reproduced with permission from ref. 119.

The new species was thus assigned to the CO^- radical anion (Figure 18) Actually, various similar species were detected in the experiment, for none of which the electron transfer is complete, the total spin density on the molecule (C+O) ranging from 0.46 to 0.62. The observed monomer CO radicals are more correctly described by the general formula $CO^{\delta-}$. As confirmed by theoretical

calculations¹²¹ the CO⁻ radical anion is unstable and reacts further with CO to give the more stable dimer C₂O₂⁻ ethyldione anion radical. The reactions observed¹¹⁹ can be described as follows:



Some ethyldione anions are stabilised at the surface, where they are observed by EPR while others react with electrons to give diamagnetic C₂O₂²⁻ ion which, in turns, undergoes a series of condensation reaction producing cyclic and linear oxycarbon dianions (C_nO_n²⁻) which have been observed by vibrational spectroscopy^{122,123}. Polymeric radical species derived from CO, and similar to those here described for MgO, have been reported on Scandium, Yttrium and Lanthanum oxides¹²⁴ and on zirconium dioxide¹²⁵.

7.3 Tetra-atomic and penta-atomic carbon containing radicals.

A number of studies have reported results on C-containing biological calcified tissues and synthetic apatites, and both bulk and surface-stabilized radicals generated by high energy irradiation were identified^{126,127}. Surface radicals are formed by interaction of the solid with atmospheric agents. They are two slightly different CO₂⁻ radical anions, characterized by large ¹³C hyperfine constants not very different from those reported in Section 7.2 and a CO₃⁻ radical anion which, differently from CO₂⁻, has a rather small ¹³C constant associated to the central atom (A₁ is unresolved, A₂ = A₃ = 13 G). This species has in fact a ground electronic state of A₂' symmetry with the unpaired electron in an antibonding orbital built up by three oxygen p orbitals. A fourth radical formed by exposure of the solid to the atmosphere and characterized by g₁ = 2.0030, g₂ = 2.0015, g₃ = 2.0023 was tentatively assigned¹²⁶ to CO⁻. This is however in contrast with the expected structure of the g tensor of this radical species which has been previously discussed in this Section.

An interesting penta-atomic carbon radical ion, isolated at the surface of various systems, is composed by one carbon and four oxygen atoms and bears one negative charge. This radical ion will be thereafter referred to as CO₄⁻. However in the first report on this species, formed by oxygen addition at 77K to a CO₂⁻ radical adsorbed on MgO, the authors described the species as the association of CO₂ to a superoxide O₂⁻ ion¹²⁸. A later report¹²⁹ described the species as a peroxy radical, because its motional behaviour and the g_{zz} value of 2.040, typical of true peroxy radicals. The hyperfine coupling constants of ¹³C (very small for all components as in the case of CO₃⁻) and

^{17}O derived from ^{17}O -enriched dioxygen (very asymmetric distribution of spin density) are in good agreement with the peroxy nature of CO_4^- . Carbon is surrounded by three oxygen atoms (small ^{13}C hyperfine) one of which is bound to the fourth oxygen to form the peroxy group. The same radical species was observed, with similar parameters, by Kazanskii and coworkers¹³⁰ on both Cr/SiO₂ and Mo/SiO₂ catalysts.

The mechanochemical approach has been successfully employed for the activation of molecules and for catalytic reactions. The mechanical energy is provided to a solid or a gas solid system *via* milling, in a given atmosphere, leading to some radical intermediates. The most interesting case is that of crystalline SiO₂ (quartz). In the early 1970's Hochstrasser and Antonini showed that upon crushing quartz, radical defects centers were formed on the cleaved surfaces which they identified as E_s' centres or $\text{Si}\cdot$, dangling bonds on the Si atom bearing the unpaired electron¹³¹. These centres, stable under ultra high vacuum, react with CO₂ forming a Si^+CO_2^- complex by partial charge transfer, exhibiting a hf coupling constant of $A(^{13}\text{C}) = 217 \text{ G}$. The mechano-chemistry of quartz surfaces was much investigated by Radtzig who proposed the existence, beside the E_s' centre of a $\text{SiO}\cdot$, an EPR silent counterpart formed upon cleavage of a Si-O-Si¹³². This could explain the formation of a $\text{SiCO}_2\cdot$ surface centres upon adsorbing CO on the surface of quartz crushed under helium^{133,134}:



In eq. 23, we have used the author's covalent vision of the chemical bond in SiO₂ but there is no doubt that the $\text{SiCO}_2\cdot$ center and the Si^+CO_2^- reported by Hochstrasser and Antonini¹³¹ are basically the same, as confirmed by the similar ^{13}C hf coupling constants (236 G obtained from a badly resolved structure for the latter case, compared to 217 G for the former). Addition of oxygen at 77K on the $\text{SiCO}_2\cdot$ radical centre leads to the $\text{SiCO}_4\cdot$ species which is the covalent form of the species discussed above as CO_4^- . This species is unstable and can be thermally decomposed producing CO₂ in the gas phase. The overall reaction is the oxidation of CO to CO₂ at the surface of quartz performed via mechanochemical activation.

Table 3 gathers the main features of the radicals discussed in this section.

8. Nitrogen containing radicals.

The chemistry of nitrogen inorganic compounds, being intimately connected to biogeochemical nitrogen cycles¹³⁵, atmospheric and environmental processes, large scale industrial processes¹³⁶ and anthropogenic pollutants abatement¹³⁷ is a cornerstone of chemical sciences. It is

not therefore surprising that nitrogen chemical species are of great importance also in interfacial chemistry in relation to the molecular activation of dinitrogen, often by heterogeneous catalysis, and to atmospheric pollution control. We focus here on surface radicals generated along processes involving essentially dinitrogen as well as nitrogen oxides. Because N_2^- and NO, are important radicals in this context, it is convenient to preliminary introduce the electronic and g tensor structures of these eleven electron radicals in some detail.

8.1. The g Tensor of 11-electron Π radicals.

Eleven electron radicals, which include CO^- discussed in the previous Section, are characterized by the presence of an unpaired electron in the π antibonding orbitals as shown in Figure 14 for NO.

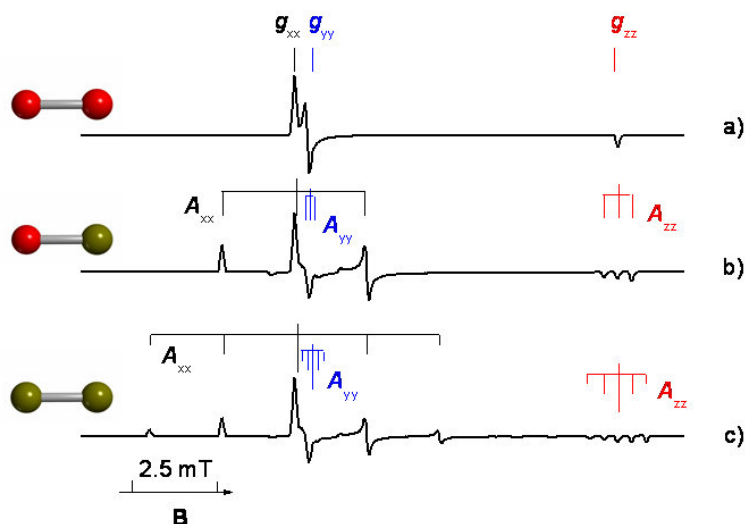


Figure 19. Simulated EPR spectra of 11 electrons Π radicals containing respectively 0 (a), 1 (b) and 2 equivalent (c) nuclei with $I = 1$.

The degeneracy of the two antibonding orbitals is lifted by the spin orbit coupling and by the asymmetric electric field, such as that exerted by a surface cation. As discussed in Section 5, this quenching effect makes EPR active a species otherwise hardly visible. The electronic configuration leads to an orthorhombic g tensor whose elements were derived by Brailsford *et al* as follows:¹³⁸

$$g_{zz} = g_e - 2\lambda\sin 2\alpha \quad (24.a)$$

$$g_{yy} = g_e\cos 2\alpha + (\lambda/E)(1 + \cos 2\alpha + \sin 2\alpha) \quad (24.b)$$

$$g_{xx} = g_e\cos 2\alpha + (\lambda/E)(\cos 2\alpha - \sin 2\alpha - 1) \quad (24.c)$$

where λ is the spin orbit coupling constant, E and Δ are the energy differences shown in Figure 14a while $\tan 2\alpha$ is defined as λ/Δ . It follows from the above equations that $g_{yy} > g_{xx} > g_{zz}$, and an important shift from g_e is expected for one component (g_{zz}) as indeed experimentally observed (Table 4). The previous equations become to first order:

$$g_{zz} = g_e - 2\lambda\Delta \quad (25.a)$$

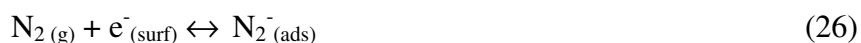
$$g_{yy} = g_e + 2\lambda E \quad (25.b)$$

$$g_{xx} = g_e \quad (25.c)$$

To illustrate the influence of the \mathbf{g} and \mathbf{A} tensors on the EPR line shape, Figure 19 gives the simulated spectra, for three hypothetical cases related to radicals with the same \mathbf{g} tensor and 0, 1 or 2 equivalent nuclei with $I = 1$. The hyperfine coupling constant values ($A_{yy} > A_{xx}, A_{zz}$) are similar to those found for radicals described in the following. One nitrogen nucleus gives a triplet of hf lines with 1:1:1 relative intensities for all directions of the \mathbf{g} tensor, while two equivalent nuclei produce a quintuplet of hf lines with 1:2:3:2:1 relative intensities.

8.2. Diatomic species: the radical anion of dinitrogen.

The nitrogen molecule is extremely stable and its chemical activation is a challenging task for both inorganic^{139,140} and bioinorganic chemists.¹⁴¹ A recent achievement in this field is the reversible reduction of dinitrogen to form the N_2^- radical anion on MgO and on CaO containing surface-trapped electrons. Beside interesting optical and magnetic properties^{142,143}, these systems show a tremendous reducing capacity. The EPR spectrum of the N_2^- radical ion is observed after nitrogen adsorption at low temperature ($T < 120\text{K}$) on the oxide electron-rich surface¹⁴⁴ and exhibits a hyperfine structure (Figure 20) using either $^{14}\text{N}_2$ or $^{15}\text{N}_2$ molecules. The features of the spectrum were computer simulated and assigned to a diatomic 11 electron $^2\Pi_{1/2}$ species with two magnetic and structurally equivalent nitrogen nuclei, namely the N_2^- radical ion,^{145,146} adsorbed on a positive ion at the oxide surface and formed as follows:



The adsorption is reversible and, by lowering the gas pressure or rising the temperature, molecular nitrogen is desorbed and the electron trapped back by the surface.

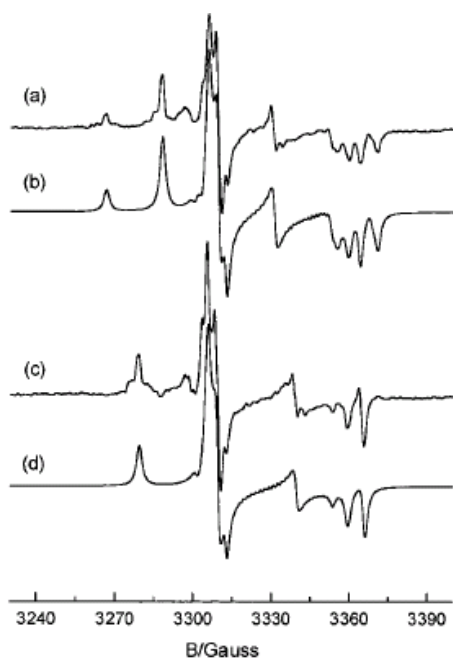


Figure 20. Experimental (77K) and computer simulated EPR spectra of $^{14}\text{N}_2^-$ (a,b) and $^{15}\text{N}_2^-$ (c,d) on MgO. Figure reproduced from ref. 145.

Analysis of the hyperfine tensor¹⁴⁵ indicates that the electron-nucleus interaction is essentially dipolar being the unpaired electron mainly confined in the π_y antibonding orbital with some admixture of the π_x . The spin density calculated with the classic procedure of comparison between the experimental and the atomic values is about 0.92 for N_2^- on MgO and 0.89 in the case of CaO. The charge transfer degree from the surface to the molecule is thus very high and the interaction is essentially ionic. It is indeed the large stabilizing contribution of the ionic interaction between a surface cation and the adsorbed radical anion to the chemical bonding that explains the electron transfer onto the N_2 molecule. The ionisation energy of the trapped electron and the electron affinity of the molecule are in fact both endothermic. The reason for the reversibility of the process is more subtle. Calculations at the DFT level^{145,147} show that the formation of the charge transfer complex is slightly exothermic (fraction of an eV according to the type of adsorption site)¹⁴⁸ and that there is a low activation energy at the crossing between the unbound ($e^-_{(\text{surf})}/\text{N}_2$) and the bound ($\text{N}_2^-_{(\text{surf})}$) states. The calculations also indicate that adsorbed N_2^- radical ion is elongated by about 8% with respect to the gas phase molecule, consistent with the occupation of an antibonding orbital by the unpaired electron and with the view of the described process in terms of a true activation of the nitrogen molecule.

8.3. Diatomic species. Nitric oxide, a multipurpose surface probe.

Nitrogen oxides (NO_x) are ubiquitous by products of high temperature combustions and very noxious pollutants of the atmosphere. Their removal from burnt gases is required in stationary installation (power plants) and in mobile sources (automotive vehicles). In the former case, nitrogen oxide abatement is achieved either by selective catalytic reduction (SCR) using various reducing agents (NH_3 , hydrocarbons or alcohols) or by direct decomposition of NO into N_2 and O_2 . This latter reaction is extremely difficult due to the enormous kinetic limitations and only recently it was discovered by Iwamoto and coworkers¹⁴⁹ that Cu/ZSM5 zeolites are active catalysts for this process. The interaction of NO with surfaces has therefore become an important field of research and has been investigated by means of a *plethora* of experimental techniques.

There is another reason that explains the interest in NO: because of its radical nature, this molecule is also often used to probe the properties of oxide surfaces and its dynamics, particularly in complex environments such as micro- and meso-porous systems (Section 5). In what follows, we will first describe the interaction of NO with cationic sites (8.3.1) as followed by EPR, then we will discuss the less common case of NO as probe of basic sites (8.3.2) and in Sec. 8.3.3 we will show how NO has been used to monitor the properties of certain transition metal ions (TMI).

8.3.1. Cationic sites.

Although NO is a most stable radical, it has remained unidentified by EPR for many years. In gas phase the molecule has a complete coupling between the electron spin \mathbf{S} and the angular momentum \mathbf{L} leading to a $^2P_{1/2}$ ground state which is not split by a magnetic field (the components of \mathbf{S} and \mathbf{L} are antiparallel so that $g_J = 0$)¹⁵⁰. The EPR spectrum recorded for gas phase NO is due to the partially populated high energy $^2P_{3/2}$ state and is observed at resonant field corresponding to $g_J = 4/5$ (0.77). When NO is in an adsorbed state, two effects allow the observation of an EPR spectrum. The former one is the quenching of the orbital momentum by the electric field of the adsorption site which causes the $^2P_{1/2}$ state to become a paramagnetic, pure spin state. The second is the lifting of the degeneracy of the two π^* orbitals producing an energy splitting Δ which determines (Figure 14, Equations 25) the g values, close to 2, of adsorbed NO.

The first EPR spectrum, dealing with MgO and recorded at 93 K by Lunsford¹⁵¹, was assigned to “an adsorbed NO molecule in a strong field at the surface such that the spin-orbit coupling is partially quenched”. The signal exhibits a structure expected for a 11 electrons Π radical with $g_{xx} = g_{yy} = 1.995$, $g_{zz} = 1.90$, $A_{xx} = 30\text{G}$ and $A_{zz} < 10\text{G}$. The surface-molecule bond however is rather weak and NO desorbs outgassing the sample at room temperature. The NO molecule is thought to weakly interact with the polarizing field of a surface Mg^{2+} cation. A number of papers followed, reporting spectra of NO adsorbed on cationic sites of ZnO and ZnS,¹⁵² Y

^{153,154,155} and A zeolites,^{156,157} Al₂O₃,¹⁵⁸ TiO₂ and SnO₂,¹⁵⁹ CeO₂.¹⁶⁰ The energy splitting parameter Δ was calculated *via* equation 25a for various systems and the values obtained show that the g_{zz} component is indeed very sensitive to the charge of the positive adsorption site, substantiating its use as probe of cationic sites.¹⁶¹

Recently the interaction of NO with MgO was revisited employing highly crystalline nanostructured materials prepared by Chemical Vapour Deposition (CVD)¹⁶². The EPR spectrum, better resolved than in earlier studies,¹⁵¹ exhibits three independent lines at high field (Figure 21a) corresponding to the g_{zz} values of NO radicals having very similar g_{xx} and g_{yy} and adsorbed on three distinct Mg²⁺ cations which, because of their different coordination state, exert different polarizing power on the molecule. The lower the coordination, the higher the strength of the electric field exerted by the cation.

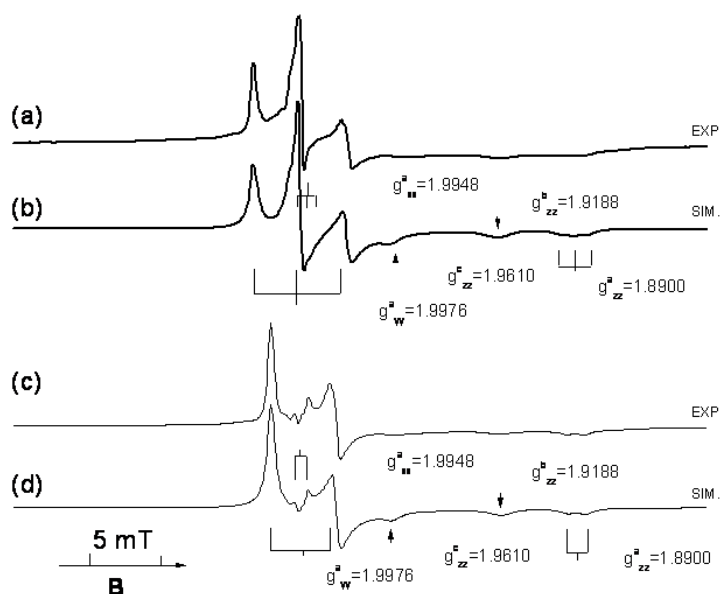


Figure 21. Experimental and computer simulated EPR spectra of adsorbed ¹⁴NO (a,b) and ¹⁵NO (c,d) on MgO. Spectra recorded at 77 K. Figure adapted from ref. 162.

This results outlines the remarkable property of NO to discriminate surface cationic sites. In the spectrum recorded using ¹⁵NO (I(¹⁵N) = 1/2) instead of ¹⁴NO (Figure 21c) each hyperfine triplet is substituted by a doublet (see for instance the component at $g = 1.8900$). Analysis of the hyperfine structure (Table 4) indicates that the total spin density on the N atom of the best resolved species is about 0.803. This remarkable localization of the spin density on the N atom is not surprising, if the prevalent nitrogen character of the antibonding orbitals in the hetero-nuclear NO molecule is taken into account. The spin density on the adsorbed molecule is very close to that of free NO confirming that the perturbation of the molecule associated to the interaction with the surface is rather weak.

The nature of the “surface – NO” interaction originally proposed by Lunsford was confirmed by theoretical calculations. The NO molecule interacts with low-coordinated Mg^{2+} cations at edges and corners. The interaction energies, in agreement with the experimental results, are weak (0.10-0.20 eV) but increase with decreasing the surface coordination of Mg^{2+} . In this bonding mode the molecule is virtually unperturbed with respect to the free molecule. On five coordinated ions at the surface the interaction energy of a single molecule is negligible and physisorbed diamagnetic $(NO)_2$ pairs are preferentially formed.

A further application of the properties of NO as surface probe was found investigating the dissociative chemisorption of H_2 on MgO. It was found that two out of the three described NO sites are involved in H_2 dissociation. As a matter of fact, they no longer lead to EPR spectra typical of adsorbed NO radicals, upon contact of NO with a surface pre-covered by hydrogen.

Pulsed techniques and high field EPR have lead to new investigations on NO complexes in zeolites aiming to describe the nature of Lewis acid sites. Though the general description of the NO weak interaction on Lewis sites is confirmed, the use of W band¹⁶³, ENDOR¹⁶⁴ and pulsed ENDOR¹⁶⁵ on Na containing ZSM-5 and A zeolites allowed the determination of previously unknown structural parameters for the Na^+NO and $Al^{3+}NO$ complexes. The NO adduct on Na^+ ions for instance has a bent structure with a Na-N-O angle of 142° . Desorption of the NO complex has also been investigated in terms of the equilibrium between the adsorbed molecule and the gaseous one. The latter was monitored via the $^2P_{3/2}$ state resonating at $g=0.77$ ¹⁶⁶.

NO coordination can lead also to di-nitrosyls complexes especially in the case of transition metal ion compounds. In some case the presence of NO di-adducts with $S=1$ (triplet state) has been observed on surfaces like in the case of zirconium dioxide¹⁶⁷ or in that of the widely studied A zeolites.^{154, 168, 169}

8.3.2. Anionic sites.

The cationic acidic sites described above are not the only ones involved in NO adsorption, basic sites also are, as reported by Lunsford.¹⁵¹ This finding was described in the paper which first illustrated the NO interaction with MgO and revisited recently.^{162,170} NO can be strongly chemisorbed on particularly basic O^{2-} sites of MgO, i.e., *via* covalent bonding and formation of the radical anion NO_2^{2-} as follows:



The above is an example of covalent bonding between a molecule and a solid surface (Fig 5b of Section 4.2b). Though a notation such that adopted here (NO_2^{2-}) is compact and easy to use, one has to realize that one of the two oxygen belongs to the solid and that, in principle, the spin density and the charge are not restricted to the sole triatomic radical. NO_2^{2-} has 19 electrons and the same electronic structure as that of the ozonide O_3^- ion. Its EPR spectrum (Figure 22a) is characterised by three g values rather close one to the other (Table 4) and a nitrogen hyperfine coupling of about 40G centred on the smaller g component. The main contribution to the hf interaction is dipolar because the odd electron is in an antibonding orbital formed from three parallel p orbitals centered on the three atoms. The non negligible contribution of the $2s$ nitrogen orbital is essentially due to spin polarisation. Theoretical calculations¹⁶² have shown that the two N-O bonds are not equivalent but both with the features typical of covalent bonding (Figure 22b). In the case of MgO, the formation of NO_2^{2-} concerns very few low coordinated O^{2-} ions, while the large majority of NO radicals is formed on surface cations, as described earlier.

The situation is completely reversed in the case of CaO¹⁷¹ which, being more basic than MgO, interacts with NO with its basic oxide ions only and not with its cations. This interaction, however, is rather complex and four distinct radical species, all formed according to equation 27, have been observed showing different stability and progressive variation of the spin density on the nitrogen atom.¹⁷¹

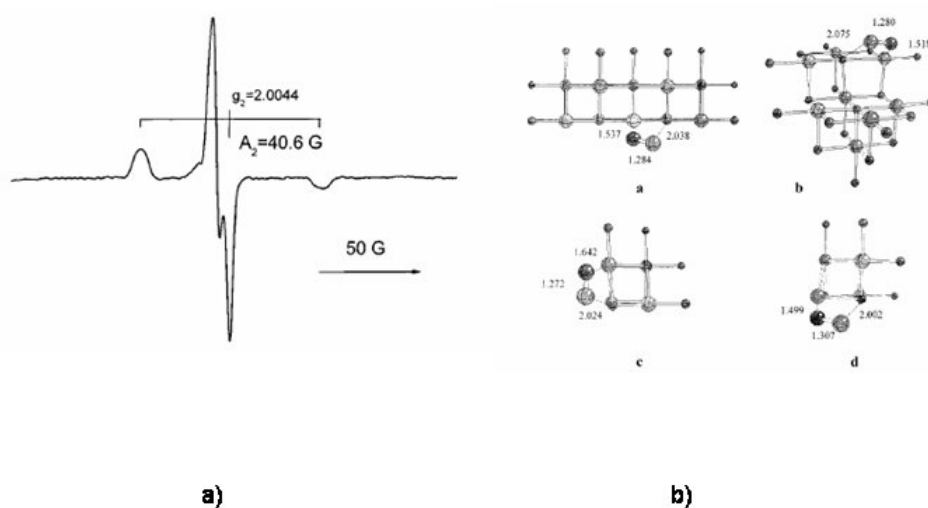


Figure 22. a) EPR spectrum of the NO_2^{2-} radical ion formed on MgO; b) computed structures of NO chemisorbed at O^{2-} anions at different surface sites. Adapted from ref. 162.

The surface O^{2-} ions involved represent around 0.5% of the total number of surface sites and are the strongest basic sites, i.e., those with low coordination number (4- and 3-coordinated O^{2-} ions at edges, corners and other morphological defects). The more abundant 5-coordinated sites present at the planar (100) faces of the cubic oxide are not concerned. The concentration of such basic sites is 25 times higher on CaO than on the less basic MgO.

Well resolved X- and Q-band EPR spectra assigned to NO_2^{2-} were also reported for TiO_2 upon calcination in air (300-450°C) of samples prepared by addition of $TiCl_4$ to water solutions containing either sodium hydroxide or ammonia followed by filtration and drying.¹⁷² The formation of NO_2^{2-} was attributed to the reaction of NO, formed by oxidation of ammonia ($4 NH_3 + 5 O_2 \rightarrow 4 NO + 6 H_2O$) with oxygen ions according to the reaction in eq. 27. NO_2^{2-} ions are located in the bulk because their EPR spectra were not broadened by excess gas phase oxygen. This explanation was substantiated by the fact that the thermal treatment *under vacuum* (instead of calcinations) did not generate the spectra assigned to NO_2^{2-} . The results show that the samples keep the memory of the ammonia preparation route leading to N-doped TiO_2 .

The same system has been revisited to prepare such samples used as photo-catalysts and the spectra were assigned¹⁷³ to a nitrogen species in interstitial sites of the bulk of TiO_2 which binds to an oxygen ion to form a NO^{2-} centre with EPR parameters close to those of NO_2^{2-} . This result was corroborated by *ab initio* calculations which proved the consistency of the experimental parameters with those expected for a N interstitial species but also suggested that reaction 27, occurring at the surface of alkaline earth oxides, cannot take place in the bulk of TiO_2 whose O^{2-} ions are not basic enough to bind NO. This example illustrates the importance of theoretical modelling in assigning EPR spectra.

8.3.3. NO as a probe of surface transition metal ions.

The weak bonding of inorganic radicals described in Section 6.3.1 with surface cations becomes more involved when the latter are Transition Metal Ions (TMI). The interaction between NO and TMIs leads to a family of adducts called nitrosyls.¹⁷⁴ Surface analogs of molecular nitrosyls are frequently observed at oxide surfaces or in zeolites in relation to catalysis work aiming at eliminating nitrogen oxides from various pollutants emission. Review papers on this subject are available in the literature.¹³⁷

The formation of a nitrosyl adduct with a TMI (in most cases two open shell systems) often involves spin pairing with important variation of the electronic structure of the system. An example of such behaviour is found in Ni^{2+} doped MgO.¹⁷⁵ The EPR spectrum of the solid, dominated by the broad signal of bulk Ni^{2+} ions in octahedral coordination ($3d^8$, high spin), is modified by

adsorption of NO. Beside the already discussed NO-Mg²⁺ signal, a novel axial signal appears ($g_{||} = 2.274$ and $g_{\perp} = 2.131$, values typical of 3d⁹ Ni²⁺ ions) related to the NO-Ni²⁺ interaction occurring with the ions located at the planar (100) face of the cubic MgO crystals (C_{4v} symmetry).

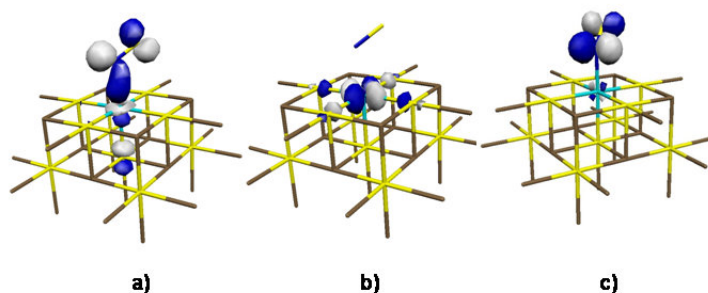


Figure 23. Three dimensional representation of relevant MO orbitals of NO/Ni²⁺MgO; a) HOMO; b) SOMO; c) lowest Unoccupied Molecular Orbital (LUMO).

The chemical bonding is determined by the interaction of the d_z^2 Ni²⁺ orbital with the π_{xz}^* orbital of NO (both singly occupied) which form a doubly occupied MO, the HOMO (Figure 23a). One unpaired electron is left in the $d_{x^2-y^2}$ orbital which becomes the SOMO and is responsible of the axial EPR signal. The Ni²⁺ ion has therefore a formal d⁹ configuration with one hole in the d shell which explains the nature of the observed EPR spectrum even though one of the d electrons is shared with the NO molecule and no effective electron transfer from the adsorbate to the solid has occurred. A similar interaction has been monitored in Fe²⁺ containing zeolites which form different nitrosyls according to the NO pressure.^{176,177}

In other cases NO-TMI interaction occurs without spin pairing and is therefore more similar to the weak adsorption described in Sections 4.2 (Fig 5d) and 6.3.1 as in the case of NO on Cu⁺ ions in various zeolites^{178,179,180} or on silica.¹⁸¹ Cu⁺ (3d¹⁰) is a closed-shell diamagnetic ion. The adsorption of NO gives the EPR-visible Cu⁺NO complex which is particularly important because it is a crucial intermediate in the decomposition of NO into N₂ and O₂ catalyzed by Cu⁺/ZSM5 zeolites.^{149,182} The presence of the copper nucleus having nuclear spin $I = 3/2$ leads to a NO spectrum with a superhyperfine structure in addition to the hyperfine one due to N with $I = 1$. The analysis of the complex X-band EPR spectrum was performed by Sojka *et al.*¹⁸³ on the basis of simulation of the spectrum. The determination of the spin-Hamiltonian parameters is particularly difficult because the axes of the g and A tensors do not coincide due to the low symmetry (C_s) of

the complex (Table 2). The Cu^+NO complex has a η^1 bent structure (Figure 24) with the unpaired electron residing mainly on the coordinated NO moiety. The large copper shf constant is actually due to the partial delocalization of this electron on the Cu 4s orbital. The total spin density on copper is found to be equal 0.2 (0.8 is on NO) and is shared among 4s (0.1), $3d_z^2$ (0.08) and $3d_{xz}$ (0.02) orbitals. Analysis of the EPR parameters allowed a thorough description of the bonding interaction which essentially involves the overlap of the two π^* orbitals of the NO molecule with the copper d orbitals of suitable symmetry.¹⁸³ This picture is fully supported by multifrequency EPR studies^{184,185,186} (Figure 24), theoretical calculations¹⁸⁷ and ENDOR¹⁸⁸ experiments.

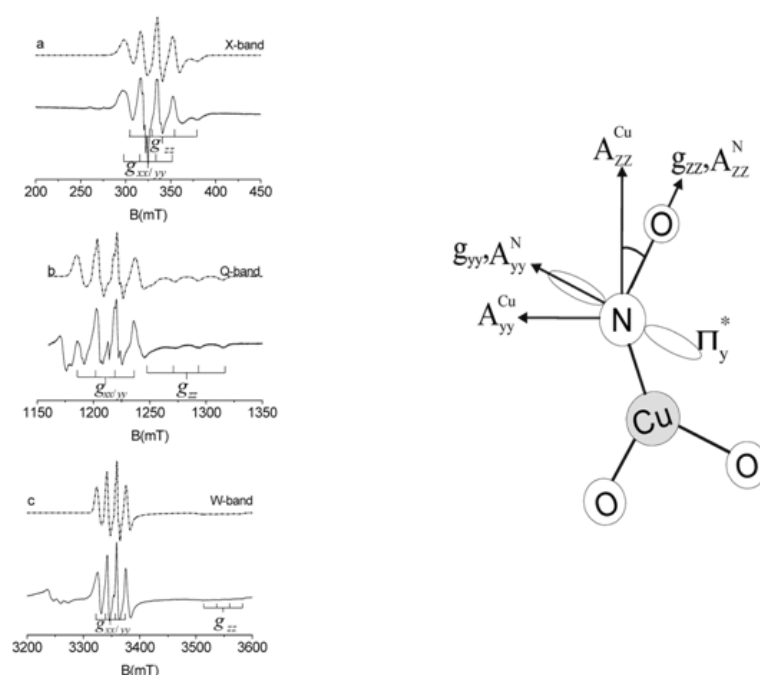


Figure 24. X band, Q band and W band EPR spectra of $\text{NO}/\text{Cu}^+\text{ZSM-5}$ system. The magnetic axes of the complex are also shown. Figure adapted from ref. 184.

8.4 Nitrogen containing triatomic surface radicals.

Triatomic radical ions derived from nitrous oxide N_2O , namely N_2O^+ and N_2O^- , have been in some case proposed,^{189,190} but their existence never unambiguously demonstrated.

Nitrogen dioxide, NO_2 , is a stable radical whose EPR spectrum in solid matrices has been widely investigated. The bent 17-electrons NO_2 molecule, isoelectronic of CO_2^- has a large nitrogen isotropic hyperfine constant (a_{iso}) due to the contribution of the N(2s) orbital to the SOMO (see Section 6.3). Nitrogen dioxide is very reactive and its use as a surface probe is limited to the case of relatively inert oxides. In such a case NO_2 is used essentially as a probe for mobility investigation

on oxide surfaces (Section 5.2) and in the channels of zeolites¹⁹¹ because it does not possess the sensitivity of NO to surface crystal field. In many other cases the NO₂ molecule reacts with oxide surfaces forming diamagnetic species (nitrates, nitrites etc.) and in few cases only, like that of MgO,¹⁹² a fraction of the molecules is adsorbed nearly unperturbed on less reactive sites.

NO₂ was employed in the first EPR investigation of a submonolayer adsorbate on a single crystal surface⁸⁶ published in 1995.

8.5 Nitrogen containing tetra-tomic and penta-atomic surface radicals.

Two tetra-atomic N-containing radical ions adsorbed on oxide surfaces have been reported, with 23 and 25 electrons respectively. The former one is the N₂O₂⁻ radical ion observed after UV irradiation at 77K of titanium dioxide dispersed on a porous glass in a N₂O atmosphere⁶⁹ (Figure 25).

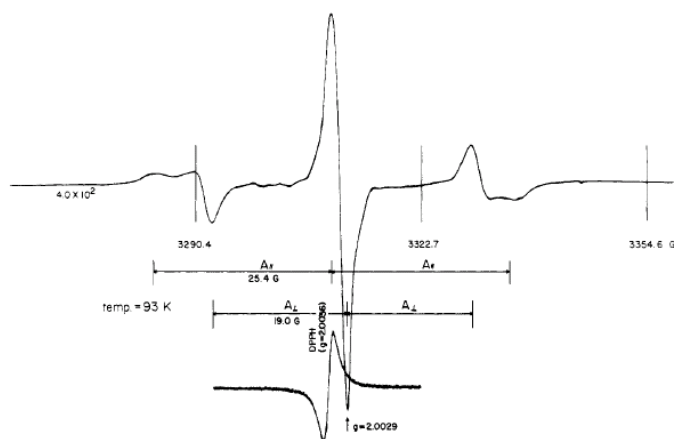


Figure 25. EPR spectrum of N₂O₂⁻ radical ion obtained with ¹⁴N¹⁵NO on TiO₂ dispersed on a porous glass. Figure reproduced from ref. 69.

The N₂O₂⁻ radical ion forms by reaction of N₂O with a photo-generated hole (eq.28) localized at the surface (Section 4.4). Surprisingly the EPR signal of N₂O₂⁻ (fig. 25) exhibits an hyperfine structure suggesting the presence of one nitrogen atom only (Table 4). However, the spectra obtained using either ¹⁴N¹⁵NO or ¹⁴N¹⁴NO are very similar one to the other, indicating that the spin density on the central N atom is negligible. The addition of N₂O on the O⁻ ion takes place at the central nitrogen atom of the molecule:



The N_2O_2^- radical anion (Fig.26a), analog of the more common CO_3^- , is expected to be planar, the unpaired electron being confined in the π antibonding orbital formed by the three outermost atoms (1N and 2O) around the central nitrogen. The spin density on this latter one is very small as indicated also by the SOMO orbital reported in Figure 26a which, though neglecting the perturbation from the solid, is consistent with the isotopic labelling result mentioned above. While the observed hyperfine structure is in line with the assignment, the g tensor of the radical should have a component greater than g_e in the direction perpendicular to the molecular plane. This seems not to be the case making the assignment open to discussion.

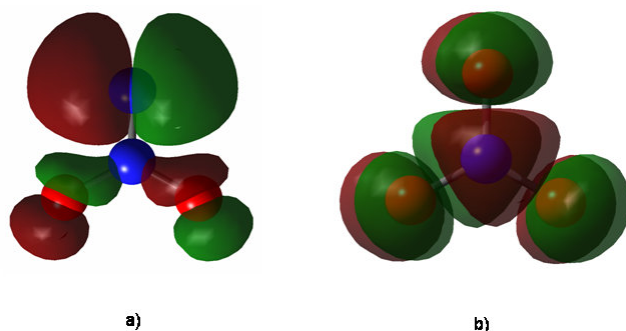


Figure 26. SOMO orbitals of N_2O_2^- (a) and NO_3^{2-} (b) radical ions in gas phase.

The formation of the 25-electrons, tetratomic NO_3^{2-} radical ion, observed in the early steps of the complex interaction of NO with the surface of activated CaO ,³⁶ is believed to involve peroxy groups (or at least of O^- pairs) capable of binding a single NO molecule following the reaction:



The species is rather unstable and its spectrum disappears after increasing the NO pressure due to the formation of nitrate groups. The EPR spectrum of NO_3^{2-} is characterised by axial g and A tensors with rather high nitrogen hyperfine coupling in both directions (Table 4) similar to those observed for the same species in irradiated KCl or KNO_3 . This tetraatomic radical ion is pyramidal (Section 6.3), the 25th electron being in an antibonding orbital (Figure 26) which acquires some s-character and becomes less antibonding with progressive bending of the structure.

The last case considered in this Section is that of a 25 electrons, pentatomic radical ion containing both carbon and nitrogen first assigned¹⁹³ to CNO_2^{2-} and finally identified as CNO_3^{2-} .¹⁹⁴

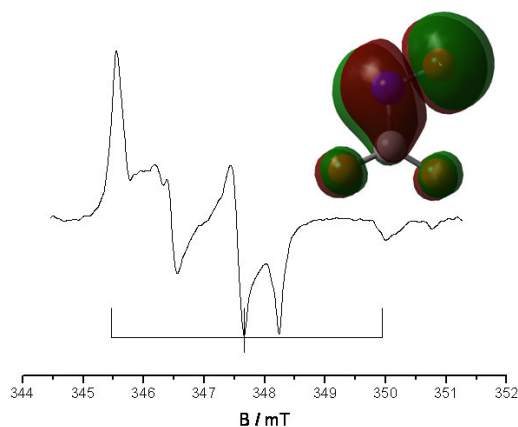
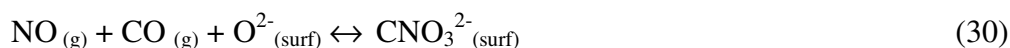


Figure 27. EPR spectrum (77K) and gas phase SOMO orbital of the CNO_3^{2-} radical anion adsorbed on MgO.

In environmental catalysis, CO and NO components found in automotive exhaust gases, are made to react to form N_2 and CO_2 . The important feature of the CNO_3^{2-} radical anion is that it is formed by coadsorption of these two gases on MgO and can thus be regarded as a reaction intermediate. Once again, the basic O^{2-} sites of MgO play a role in binding one of the molecules (CO) forming an initial surface complex (CO_2^{2-}) capable of NO addition, as follows:



The assignment of this radical ion was done on the basis of both a systematic isotopic substitution (spectra with ^{12}C , ^{13}C , ^{14}N and ^{15}N were obtained) and comparison with the infrared spectra of the same radical¹⁹³. The structure of CNO_3^{2-} is similar to that of CO_4^- (Section 7.3) with a carboxy group in contact with the surface and a NO group on top of it with bent geometry¹⁹⁵ (Figure 27). The spin density is mainly confined on the three terminal (CNO) atoms with a smaller contribution of the two carboxylic oxygens.

9. Sulphur and chlorine containing radicals.

The chemistry of sulphur compounds adsorbed on oxide surfaces plays an important role in hydrodesulphurisation catalytic reactions. Significant information on the chemical nature of sulphur containing radical intermediates and on their structure have been derived, particularly in the few studies performed using molecules enriched in the ^{33}S isotope ($I=3/2$). The natural abundance of this isotope (0.76%) is not sufficient to give detectable hyperfine structures using non enriched materials.

The only report available concerning the S_2^- dimer radical (analog of O_2^-) is due to Kazansky and coworkers¹⁹⁶ who observed well resolved X- and K-band EPR spectra upon treatment of MoO_3/SiO_2 and MoO_3/Al_2O_3 catalysts with ^{33}S enriched H_2S at 573K. The g tensor of the species is rhombic with $g_1=2.048$, $g_2=2.029$, $g_3=1.998$. The hyperfine structure is due the overlap of the quartet related to the $^{33}S-^{32}S^-$ isotopomer with the seven lines structure of $^{33}S-^{33}S^-$. The assignment of the species is mainly done on the basis of the g tensor while the electron spin density distribution was not discussed.

Triatomic negative sulphur and sulphur-oxygen monoanions were observed at the surface of MgO by Lunsford and coworkers for all the possible compositions (SO_2^- , S_2O^- , S_3^-). All these radical ions bear 19 valence electrons. In spite of their similarity they were obtained by different chemical routes.

SO_2^- can be formed by electron transfer from trapped electrons to SO_2 on MgO ¹⁹⁷. The radical ion (previously investigated in γ irradiated solid dithionite¹⁹⁸ or generated by electrochemical methods¹⁹⁹) was investigated in its adsorbed form using ^{33}S and ^{17}O -enriched reactants. This has allowed to derive the electron density distribution and the radical structure. The unpaired electron occupies a $2b_1''$ molecular orbital formed by the three parallel p orbitals of the sulphur and of the two oxygen atoms. The radical ion is similar to the ozonide anion (Section 4.2, Figure7) but, due to the different energy level of the involved orbitals (3p and 2p for S and O respectively) the electron spin density is mainly concentrated on the S atom (which bears from 0.71 to 0.75 of the total spin density in the case of the two main species observed). An earlier observation of the SO_2^- adsorbed radical is due to Kazanskii²⁰⁰ and coworkers to explain the EPR spectrum obtained by adsorption of SO_2 on pre-reduced TiO_2 . In another case SO_2^- was produced by electron transfer from adsorbed superoxide ions (O_2^-) to SO_2 in the channels of Y zeolites²⁰¹

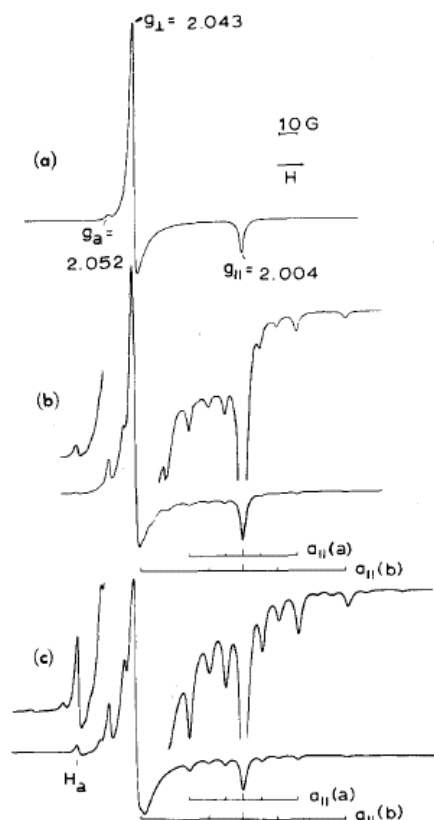
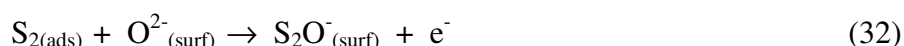
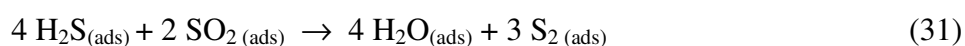


Figure 28. X-band EPR spectrum of S_3^- on MgO at different enrichment of ^{33}S . Figure reproduced with permission from ref. 203.

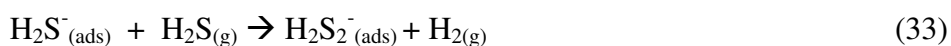
The S_2O^- radical anion was observed after surface reaction of H_2S with SO_2 . The assignment of the rhombic spectrum, very similar to that of SO_2^- , was made using, in distinct experiments, ^{33}S enriched H_2S and SO_2 respectively. The two sets of hyperfine lines indicate the presence of two non equivalent S atoms in the species. The chemical process is based on the reaction of H_2S and SO_2 producing water and S_2 . The diatomic species then reacts with a surface oxygen ion yielding S_2O^- and releasing an electron:²⁰²



The S_3^- radical ion²⁰³ origins by reaction of elemental sulphur with partially hydroxylated MgO at 400K. A sharp axial spectrum is observed using non enriched sulphur whose principal g values are $g_{\perp}=2.043$ and $g_{\parallel}=2.004$. Around these features, a complex hyperfine structure (with primary, secondary and tertiary splittings) can be analyzed on the basis of two distinct coupling constants (Figure 28). The 2:1 ratio for the two quartets indicates that there are twice as many atoms of one type with respect to the other thus allowing an unambiguous assignment of the spectrum to a

trimeric entity, the S_3^- radical ion. A complex reaction was proposed to explain the formation of the radical based on the reaction of S with surface OH groups.²⁰³

Other adsorbed sulfur-containing radicals, which include CS_2^- , COS^- and $H_2S_2^-$, were formed on MgO by transfer of surface-trapped electrons to the diamagnetic parent molecules. The first and the second type of radical ion, analogs of CO_2^- , were formed from either CS_2 or COS ²⁰⁴. The third type of radical ion obtained from H_2S is formed by a complex reaction.²⁰⁵ The first intermediate (H_2S^-) in fact further reacts with H_2S to form $H_2S_2^-$ with hydrogen desorption



The unpaired electron in this unusual radical species is thought to be localized in σ_{3p}^* antibonding orbital between the two sulphur atoms.

In a recent paper Livraghi *et al.*²⁰⁶ reinvestigated the electron transfer reaction leading to CS_2^- on the electron rich MgO surface, following the process at temperatures above those used by Lin *et al.*²⁰⁴ The authors reported a series of spectra due to the fragmentation of carbon sulphide at the surface. The mechanism, starting from the formation of CS_2^- , continues with its cleavage and formation of CS and S^- . The latter radical ion entails an oligomerisation reaction with formation of a mixture of S_n^- radical ions with $n \geq 3$ quite similar to species already observed in frozen solutions of sulphur.

While halogen containing radicals play an important role in the field of solid state defects, very few examples are reported of such radicals in adsorbed state and they concern chlorine species in zeolites. Gardner and coworkers reported the EPR spectra of ClO_2 and of Cl_2^- adsorbed in the framework of faujasite and mordenite.²⁰⁷ ClO_2 is paramagnetic and its spectrum is simply observed after adsorption in the zeolite channels. The spectrum of the 19-electron radical molecule (Section 6.3), characterised by a rhombic g tensor and by a hyperfine coupling due to the Cl atom (the largest component has a constant of about 75 G) is perturbed by the inner electric fields of the zeolitic framework which cause an increase of the Cl coupling constant.

Cl_2^- radical ions are observed after Cl_2 adsorption in the same microporous solids and subsequent γ irradiation. Cl_2^- , a σ radical having the unpaired electron in a σ^* antibonding orbital, has been widely investigated in irradiated alkali chlorides. Cl_2^- forms upon localisation of an electron hole on an anion pair ($Cl^- - Cl^-$) in correspondence of a cation vacancy.²⁰⁸ The complex hyperfine structure of Cl_2^- is due to the presence of two equivalent Cl atoms ($I=3/2$). This radical is an interesting example of a hyperfine pattern whose features are determined by the presence of different isotopomers. Chlorine has in fact two magnetic nuclei ^{35}Cl and ^{37}Cl whose natural

abundance are 75 and 25 % respectively. Both have nuclear spin $I=3/2$ but different nuclear magnetic moments and thus origin distinct hyperfine structures.

An interesting process involving chlorine dioxide was reported by Raghunathan and Sur,²⁰⁹ which elegantly showed, by EPR, the photoisomerisation of ClO_2 obtained by UV irradiation after adsorption in cancrinite. The chlorine dioxide OClO molecule in this conditions transform into ClOO , the chloroperoxy radical. The transformation dramatically changes the hyperfine structure of the molecule because most spin density in ClO_2 is on the central O atom. The main chlorine coupling constant in the chloroperoxy isomer is therefore about one order of magnitude lower with respect to the value observed for chlorine dioxide.

10. Conclusions

The role of surface inorganic radicals and radical ions formed at the interface between a solid and a gas phase has been discussed in the present review. The formation of such species is relevant to a number of fields, including electrochemistry, heterogeneous catalysis, photo-catalysis and corrosion phenomena. Identification and characterization of surface radicals are essentially conducted using Electron Paramagnetic Resonance (EPR) techniques which provide, on the basis of g , hyperfine and superhyperfine tensors, a detailed understanding of the radical composition, structure and, in some cases, of the nature of the surface adsorption sites. The first part of the review has been devoted to a methodological approach aiming both at clarifying the genesis of radical intermediates in surface processes and at evidencing their importance in typical catalytic and photo-catalytic phenomena. Furthermore, the two experimental approaches typical of EPR (direct monitoring of paramagnetic sites and use of paramagnetic molecules to probe the properties of diamagnetic systems) have been described with particular attention to the unsurpassed ability of EPR in describing motional behaviours. The second part is devoted to a systematic analysis of inorganic radicals and radical ions reported in the literature, providing careful guidelines for deriving structural information from the experiments. The main types of systems discussed, classified on the basis of the number of valence electrons, are gathered in Table 5 with essential information on their structure and ground state.

Acknowledgements

The present review is dedicated to Prof. Jack H. Lunsford a pioneer in the scientific area here described.

We gratefully acknowledge Prof. Piero Ugliengo for assistance in the computation of the SOMO orbitals. One of us (E.G.) wishes to thank the P. et M. Curie University (Paris 6) for granting a position of invited professor during the preparation of this work.

Tables

Table 1. Characteristics of the microwaves employed in EPR experiments

BAND	L	S	X	K	Q	W
Frequency ν/GHz	1	3	9.7	24	34	94
Wavelength λ/cm	30	10	3	1.25	0.88	0.32
Energy $E/\text{kJ mol}^{-1}$	$4 \cdot 10^{-4}$	$1.2 \cdot 10^{-3}$	$3.9 \cdot 10^{-3}$	$9.5 \cdot 10^{-3}$	$1.35 \cdot 10^{-2}$	$3.74 \cdot 10^{-2}$

Table 2. Relationship between EPR symmetry and molecular point symmetry of paramagnetic centres. Adapted from ref. 22.

EPR Symmetry	Relation between \mathbf{g} and \mathbf{A} tensors	Coincidence of tensor axes	Molecular point symmetry
Isotropic	$g_{xx}=g_{yy}=g_{zz}$ $A_{xx}=A_{yy}=A_{zz}$	All coincident $\alpha=\beta=\gamma=0^\circ$	O_h, T_d, O, T_h, T
Axial	$g_{xx}=g_{yy}\neq g_{zz}$ $A_{xx}=A_{yy}\neq A_{zz}$	All coincident $\alpha=\beta=\gamma=0^\circ$	$D_{4h}, C_{4v}, D_4, D_{2d}, D_{6h}$ $C_{6v}, D_6, D_{3h}, D_{3d}, C_{3v},$ D_3
Rhombic	$g_{xx}\neq g_{yy}\neq g_{zz}$ $A_{xx}\neq A_{yy}\neq A_{zz}$	All coincident $\alpha=\beta=\gamma=0^\circ$	D_{2h}, C_{2v}, D_2
Axial non-collinear	$g_{xx}=g_{yy}\neq g_{zz}$ $A_{xx}=A_{yy}\neq A_{zz}$	Only g_{zz} and A_{zz} coincident. $\alpha\neq 0^\circ; \beta=\gamma=0^\circ$	$C_3, S_6, C_4, S_4, C_{4h}, C_6,$ C_{3h}, C_{6h}
Monoclinic	$g_{xx}\neq g_{yy}\neq g_{zz}$ $A_{xx}\neq A_{yy}\neq A_{zz}$	One axis of \mathbf{g} and \mathbf{A} coincident. $\alpha\neq 0^\circ; \beta=\gamma=0^\circ$	C_{2h}, C_s, C_2
Triclinic	$g_{xx}\neq g_{yy}\neq g_{zz}$ $A_{xx}\neq A_{yy}\neq A_{zz}$	All axes non coincident $\alpha\neq\beta\neq\gamma\neq 0^\circ$	C_1, C_i

Table 3. Spin Hamiltonian parameters of Carbon containing surface paramagnetic species.

Radical species	Solid	g Tensor			A Tensor (^{13}C)/Gauss			A Tensor (^{17}O)/Gauss			Notes	Ref.
		g_1	g_2	g_3	A_1	A_2	A_3	A_1'	A_2'	A_3'		
CO_2^-	MgO	2.0026	2.0009	1.9965	181	224	177	24	60	25	The reported values refer to the most abundant of three slightly different species	109
	ZrO ₂	EPR spectra reported without detailed parameters										67,68
	SiO ₂	2.0031	2.0012	1.9977	unres	236	unres					113
	Apatite	2.0030	2.0015	1.9970	164	199	159					126,127
$\text{CO}^{\delta-}$ (CO^-)	MgO	2.0041	2.0014	1.9917	-	25.3	-	-	44.5	-	The reported species is the most abundant of four slightly different species . The average value for δ is about 0.6.	119
C_2O_2^-	MgO	2.0060	2.0050	2.0021	7.8	8.4	19.0				Two equivalent C atoms (ethylendione anion). Assigned to cyclic $\text{C}_6\text{O}_6^{3-}$ in ref 7.	116-119
	CaO	2.0063	2.0048	2.0023	$A_{\text{average}} = 11.8$							
CO_3^-	Apatite	2.0170	2.0084	2.0060	unres	13.0	13.0					126
CO_4^-	MgO,	2.0040	2.0072	2.0015	unres	3.5	2.8	unres	unres	100	Peroxy radical type (O_2COO). Two inequivalent terminal O	128
	Cr/SiO ₂ , SiO ₂							unres	unres	50		

Table 4. Spin Hamiltonian parameters of nitrogen containing surface paramagnetic species .

Radical species	Solid	g Tensor			A Tensor (¹⁴ N)/Gauss			A Tensor (¹⁵ N)/Gauss			Notes	Ref.
		<i>g</i> ₁	<i>g</i> ₂	<i>g</i> ₃	<i>A</i> ₁	<i>A</i> ₂	<i>A</i> ₃	<i>A</i> ₁	<i>A</i> ₂	<i>A</i> ₃		
N ₂ ⁻	MgO	2.0018	2.0042	1.9719	2.90	21.50	4.20	4.06	30.10	5.88		144-146
	CaO	2.0006	2.0048	1.9677	2.50	20.00	4.30	3.50	28.00	6.02		
NO	MgO	1.9948	1.9980	1.8900	32.0	2.57	8.96	44.8	3.60	12.4		151,161,162
	ZnO, TiO ₂ , ZnS, Al ₂ O ₃ , SnO ₂ , CeO ₂ , Y zeolites										All spectra have structure similar to that of the spectrum reported in detail for MgO	151-160
NO ²⁻	TiO ₂	2.0054	2.0036	2.0030	2.3	4.4	32.3					173
NO ₂ ²⁻	MgO	2.010	2.0044	2.0078	unres.	40.6	unres	unres	56.8	unres		161
	CaO	2.008	2.0075	2.0080	0.5	33.0	0.5					171
NO ₂	Na/mordenite	2.0051	1.9910	2.0017	51.0	48.0	66.0					191
N ₂ O ₂ ⁻	TiO ₂ /PVG	2.0034	2.0029	2.0029	25.5	19.0	19.0				Hyperfine values are related to the external N atom. The central atom has A<2G	190
NO ₃ ²⁻	CaO	2.0057	2.0055	2.0055	61.7	41.0	41.0					36

Table 5. Molecular radical species adsorbed at solid surfaces.

Number of atoms	Number of electrons	Formula of the species	Structure	Ground state of the free radical or Symmetry of SOMO	Notes
2	11	CO ⁻		² Π _{1/2}	Quenched diatomic molecules Crystal field sensitive
		NO			
		N ₂ ⁻			
	13	O ₂ ⁻		² Π _{3/2}	Quenched diatomic molecules Crystal field sensitive
		NO ²⁻			
		ClO			
15	Cl ₂ ⁻		² Σ _{1/2}	Crystal field insensitive	
3	17	CO ₂ ⁻	Bent, C _{2v} symmetry	² A ₁	Contribution of 2s to the SOMO. Isotropic hyperfine expected. Crystal field insensitive
		NO ₂			
	19	O ₃ ⁻	Bent	² B ₁	Π system Weak isotropic coupling by spin polarisation.
		SO ₂ ⁻			
		NO ₂ ²⁻			

		ClO ₂			Crystal field insensitive
		ClOO	Bent		Peroxy type species
4	21	C ₂ O ₂ ⁻	Linear		
	23	N ₂ O ₂ ²⁻	Planar	² A' ₂	Π system Small spin density on the central atom.
		CO ₃ ⁻	Planar D _{3h}		
	25	NO ₃ ²⁻	pyramidal	² A ₁	Isotropic and anisotropic couplings from the central atom
5	29	CO ₄ ⁻			Pseudo peroxy radical (O ₂ COO)
		CNO ₃ ²⁻			Pseudo nitroxide (O ₂ CNO) ²⁻

Biographical sketches

Elio Giamello, born in 1950, is Full Professor of Inorganic Chemistry at the University of Torino since 1999. In the same university he is presently director of the Ph.D. School in Sciences and High Technology. He has been active since the early eighties, in the field of surface chemistry of metal oxides devoting particular attention to the applications of Electron Paramagnetic Resonance spectroscopy (EPR) to this field. Focus of his interest are the paramagnetic centres (defects, reactive intermediates, transition metal centres) at the surface and their reactivity. He has for three times covered the position of Invited Professor at the P. et M. Curie University (Paris VI). In 2007 he has been elected the recipient of an Humboldt Research Award by the Alexander von Humboldt Stiftung, Germany, for his scientific activity in the field of surface chemistry.



Mario Chiesa received his Chemistry degree from the University of Torino (Italy). He then moved to the University of Cardiff (U.K) with the support of a Marie Curie fellowship and in 2001 obtained his Ph.D. in Chemistry under the guidance of Dr. Damien Murphy. Currently he is Assistant Professor (Ricercatore) at the Department of Chemistry of the University of Torino. His main scientific interests are concerned with the application of Electron Paramagnetic Resonance techniques to the study of inorganic solids and interfacial phenomena occurring at their surfaces.



Michel Che was born in Lyon, France completed his doctorate (EPR study of titanium dioxide) in 1968 at the University of Lyon and studied as postdoctoral fellow at Princeton University (1969-1971). He was appointed Professor at University of Paris VI: Pierre et Marie Curie in 1975 and Senior Member of the Institut Universitaire de France in 1995. His work has led to around 400 publications in international journals. He has been very active in the promotion and organisation of catalysis, being the President-Founder of EFCATS (European Federation of Catalysis Societies) with creation in 1993 of the cycle of the now famous biennial “EuropaCat” congresses, and President of IACS (International Association of Catalysis Societies) in 2000-2004, culminating with the organisation and opening of the 13th International Congress on Catalysis held in Paris in 2004. His research activity has been largely devoted to catalysis processes involving gas-solid, liquid-solid and solid-solid interfaces. He has pioneered a molecular approach to heterogeneous catalysis, based on transition elements taken as probes, specific isotopes and physical techniques, which endows him with an original position in the field. His work has led to the emergence of interfacial coordination chemistry at the junction of colloidal, electro-, supramolecular, geo- and solid-state chemistries.



-
- (1) Atkins, P. W.; Symons, M. R. C. *The Structure of Inorganic Radical*; Elsevier: Amsterdam, 1967.
 - (2) Weltner, W.J. *Magnetic Atoms and Molecules*; Dover Publications Inc.: New York, 1989.
 - (3) Corma, A. *Chem. Rev.* **1997**, 97, 2373.
 - (4) Garcia, H.; Roth, H. D. *Chem. Rev.* **2002**, 102, 3947.
 - (5) Dyrek, K.; Che, M. *Chem. Rev.* **1997**, 97, 305.
 - (6) Sojka, Z.; Che, M. *Colloids Surf.* **1999**, 158, 165.
 - (7) Che, M.; Tench, A. J. *Adv. Catal.* **1982**, 31, 77.
 - (8) Che, M.; Tench, A. J. *Adv. Catal.* **1983**, 32, 1.
 - (9) Fubini, B.; Hubbard, A. *Free Rad. Biol. Med.* **2003**, 34, 1507.
 - (10) Janzen, E. G. In *Free Radicals in Biology*; Pryor W.A. Ed.; Academic Press, New York, 1980.
 - (11) Giamello, E. *Catal. Today* **1998**, 41, 239.
 - (12) Both radicals and paramagnetic species possess unpaired electrons. The difference between the two terms depends on their reactivity. Radicals are usually very reactive, paramagnetic species not necessarily. $\text{CH}_3\cdot$ and Cu^{2+} both possess an unpaired electron ($S = 1/2$) but $\text{CH}_3\cdot$ only is a radical.
 - (13) Adrian, F. J. *Colloid Interf. Sci* **1968**, 26, 317.
 - (14) Lunsford, J.H. *Adv. Catal.* **1972**, 22, 265.
 - (15) Howe R. F. *Colloids Surf.* **1993**, 7, 353.
 - (16) Che, M.; Giamello, E. In *Catalyst Characterization: Physical Techniques for Solid Materials*; Imelik B.; Vedrine J. C. Eds; Plenum Press: New York, **1994**.

-
- (17) Schweiger, A. *Angew. Chem. Int. Ed. Engl.* **1991**, 30, 265.
- (18) Schweiger, A. *Appl. Mag. Reson.*, **1993**, 5, 229.
- (19) Schweiger, A.; Jeschke, G. *Principles of Pulse Electron Paramagnetic Resonance*; Oxford University Press: Oxford, 2001.
20. Xu, J.; Kevan, L. *Appl. Mag. Res.* **2001**, 20, 3.
- (21) Goldfarb, D.; Bernardo, M.; Strohmaier, K.G.; Vaughan, D. E. W.; Thomann, H. *J. Am. Chem. Soc.* **1994**, 117, 6344.
- (22) Mabbs, F. E.; Collison, D. *Electron Paramagnetic Resonance of d Transition Metal Compounds*; Elsevier: Amsterdam, 1992.
- (23) Schmidt, J.; Risse, T.; Hamann, H.; Freund, H. J. *J. Phys. Chem. B* **2002**, 116, 10861.
- (24) Futako, W.; Umeda, T.; Nishizawa, M.; Yasuda, T.; Isoya, J.; Yamasaki, S. *J. Non-Crystalline. Solids*, **2002**, 299, 575.
- (25) Sterrer, M.; Fischbach, E.; Risse, T.; Freund, H. J. *Phys. Rev. Lett.* **2005**, 94, 186101.
- (26) Chiesa, M.; Giamello, E.; Di Valentin, C.; Pacchioni, G. *Chem. Phys. Lett.* **2005**, 403, 124.
- (27) The spectroscopic behavior of powders is also shown by glasses containing paramagnetic centers.
- (28) Rist, G. H.; Hyde, J. S. *J. Chem. Phys.* **1970**, 52, 4633.
- (29) Rieger, P. H. In *Specialist Periodic Reports. Electron spin resonance*; Royal Society of Chemistry: Cambridge 1993; Vol. 13B, pp 178-199.
- (30) The presence of an O⁻ ion at the oxide surface can derive from photogeneration or, alternatively, from charge compensation of an impurity (es Na⁺ in CaO).
- ³¹ Anpo, M.; Che, M.; Fubini, B.; Garrone, E.; Giamello, E.; Paganini, M.C. *Top. Catal.* **1999**, 8, 189.
- (32) Lunsford, J.H. EPR Methods in Heterogeneous Catalysis. In *Catalysis. Science and Technology*; Anderson, J.R.; Boudart, M., Eds., Springer Verlag: Berlin 1987; Vol. 8, pp 227-256.
- (33) Sojka, Z.; Giamello, E.; Paganini, M. C. Radicals in Catalysis.- Heterogeneous. In *Encyclopedia of Catalysis*, John Wiley & Sons: Chicister, 2002.
- (34) Chiesa, M.; Giamello, E.; Paganini, M.C.; Sojka, Z. *J. Chem. Phys.* **2002**, 116, 4266.
- (35) Ricci, D.; Pacchioni, G.; Sushko, P. V.; Shluger, A. L. *Surf. Sci.* **2003**, 542, 293.
- (36) Paganini, M.C.; Chiesa, M.; Dolci, F.; Martino, P.; Giamello, E. *J. Phys. Chem. B* **2006**, 110, 11918.
- (37) Kon, M. Ya.; Shvets, V. A.; Kazansky, V.B. *Kinet. Katal.* **1973**, 14, 403.
- (38) Aika, K. I.; Lunsford, J. H. *J. Phys. Chem.* **1978**, 82, 1794.
- (39) Liu, H. F.; Liu, R. S.; Johnson, R. E.; Lunsford, J. H. *J. Am. Chem. Soc.* **1984**, 106, 4117.
- (40) Bonneviot, L.; Olivier, D.; Che, M. *J. Mol. Catal.* **1983**, 21, 415.
- (41) Driscoll, D. J.; Martir, W.; Wang, J. X.; Lunsford, J. H. *J. Am. Chem. Soc.* **1985**, 107, 58.
- (42) Wang, J. X.; Lunsford, J. H. *J. Am. Chem. Soc.* **1986**, 90, 5883.
- (43) Driscoll, D.J.; Campbell K. D.; Lunsford, J. H. *Advan. Catal.* **1987**, 35, 139.
- (44) Schmidt, J.; Risse, T.; Hamann, H.; Freund, H-J. *J. Chem. Phys.* **2002**, 116, 10861.
- (45) Risse, T.; Schmidt, J.; Hamann, H.; Freund, H-J. *Angew. Chem. Int. Ed.* **2002**, 41, 1517.
- (46) *Photocatalysis: Fundamentals and Applications*; Serpone, N.; Pelizzetti, E, Eds; Wiley & Sons: Chicister, 1989.
- (47) Thompson, T. L.; Yates, J. T. *Chem. Rev.* **2006**, 106, 4428.
- (48) Kudo, A.; Miseki, Y. *Chem. Soc. Rev.* **2009**, 38, 253.
- (49) Honda, K.; Fujishima A. *Nature* **1972**, 238, 37.
- (50) Howe, R. F.; Grätzel, M. *J. Phys. Chem.* **1987**, 91, 3906.
- (51) Grätzel M.; Howe, R.F. *J. Phys. Chem.* **1990**, 94, 2566.
- (52) Nakaoka, Y.; Nosaka, Y. *J. Photochem. Photobiol. A: Chem.* **1997**, 110, 299.
- (53) Hurum, D.C.; Gray, K.A.; Rajh, T.; Thurnauer, M.C. *J. Phys. Chem. B* **2005**, 109, 977.
- (54) Ke, S.C.; Wang, T.C.; Wong, M.S.; Gopal, N.O. *J. Phys. Chem. B* **2006**, 110, 11628.
- (55) Hurum, D.C.; Agrios, A.G.; Crist, S.E.; Gray, K.A.; Rajh, T.; Thurnauer, M.C. *J. Electron Spectr. Rel. Phenom* **2005**, 109, 977.
- (56) Soria, J.; Sanz, J.; Sobrados, I.; Coronado, J. M.; Fresno, F.; Hernandez-Alonso, M.D. *Catal. Today* **2007**, 129, 240.
- (57) Berger, T.; Sterrer, M.; Diwald, O.; Knözinger, E.; Panayotov, D.; Thompson, T. L.; Yates, J. T. *J. Phys. Chem. B*, **2005**, 109, 6061.
- (58) Berger, T.; Sterrer, M.; Diwald, O.; Knözinger, E. *ChemPhysChem.* **2005**, 6, 2104.
- (59) Sterrer, M.; Berger, T.; Diwald, O.; Knözinger, E. *J. Am. Chem. Soc.* **2003**, 125, 195.
- (60) Berger, T.; Diwald, O.; Knözinger, E.; Napoli, F.; Chiesa, M.; Giamello, E. *Chem. Phys.* **2007**, 339, 138.
- (61) Anpo, M.; Shima, T.; Kodama, S.; Kubokawa, Y. *J. Phys. Chem.* **1987**, 91, 4305.
- (62) Dimitrijevic, N.M.; Saponjic, N.C.; Rabatic, B.M.; Poluektov, O.G.; Rajh, T. *J. Phys. Chem. C* **2007**, 111, 14597.
- (63) Coronado, J.M.; Soria, J. *Catal. Today* **2007**, 123, 37.
- (64) Murata, C.; Hattori, T.; Yoshida, H. *J. Catal.* **2005**, 231, 292.

-
- (65) Bedilo, A.F.; Plotnikov, M.A.; Mezentseva, N.V.; Volodin, A.M.; Zhidomirov, G.M.; Rybkin, I.M.; Klabunde, K.J. *Phys. Chem. Chem. Phys.* **2005**, *7*, 3059.
- (66) Teramura, K.; Tanaka, T.; Ishikawa, H.; Kohno, Y.; Funabiki, T. *J. Phys. Chem. B* **2004**, *108*, 346.
- (67) Kohno, Y.; Tanaka, T.; Funabiki, T.; Yoshida, S. *Phys. Chem. Chem. Phys.* **2000**, *2*, 2635.
- (68) Kohno, Y.; Tanaka, T.; Funabiki, T.; Yoshida, S. *Phys. Chem. Chem. Phys.* **2000**, *2*, 5771.
- (69) Anpo, M.; Aikawa, N.; Kubokawa, Y.; Che, M.; Louis, C.; Giamello, E. *J. Phys. Chem.* **1985**, *89*, 5689.
- (70) Giamello, E.; Garrone, E.; Ugliengo, P. *J. Chem. Soc. Faraday Transaction I* **1989**, *85*, 1373.
- (71) Giamello, E.; Garrone, E.; Ugliengo, P.; Che, M.; Tench, A. *J. Chem. Soc. Faraday Transaction I* **1989**, *85*, 3987.
- (72) Chiesa, M.; Paganini, M.C.; Giamello, E.; Di Valentin, C.; Pacchioni, G. *Acc. Chem. Res.* **2006**, *39*, 861.
- (73) Chiesa, M.; Paganini, M.C.; Spoto, G.; Giamello, E.; Di Valentin, C.; Del Vitto, A.; Pacchioni, G. *J. Phys. Chem. B* **2005**, *109*, 7314.
- (74) Chiesa, M.; Paganini, M. C.; Giamello, E.; Murphy, D.M. *J. Phys. Chem. B* **2001**, *105*, 10457.
- (75) Freed, J. H. In *Spin labelling: Theory and Applications*; Berliner, L. J., Ed.; Academic Press: New York, 1976; Vol.1.
- (76) Yahiro, H.; Lund, A.; Shiotani, M. *Spec. Acta A* **2004**, *60*, 1267 and references therein.
- (77) Shiotani, M.; Moro, G.; Freed, J. *J. Chem. Phys.* **1981**, *74*, 3757.
- (78) Nilges, M.; Shiotani, M.; Yu, C. T.; Barkley, G.; Kera, Y.; Freed, J. *J. Chem. Phys.* **1980**, *73*, 588.
- (79) Shiotani, M.; Freed, J. *J. Chem. Phys.* **1981**, *85*, 3873.
- (80) Iwaizumi, M.; Kubota, S.; Isobe, T. *Bull. Chem. Soc. Jpn.* **1971**, *44*, 3227.
- (81) Kasai, P.H.; Weltner, Jr., W.; Whipple, E.B. *J. Chem. Phys.* **1964**, *42*, 1120.
- (82) McDowell, C.A.; Nakajima, H.; Raghunathan, P. *Can. J. Chem.* **1970**, *48*, 805.
- (83) Myers, G.H.; Easley, W.C.; Zilles, B.A. *J. Chem. Phys.* **1970**, *53*, 1181.
- (84) Beckendorf, M.; Katter, U.J.; Schlienz, H.; Freund, H-J. *J. Phys. Condens. Matter* **1993**, *5*, 5471.
- (85) Beckendorf, M.; Katter, U.J.; Risse, T.; Schlienz, H.; Freund, H-J. *J. Phys. Chem.* **1996**, *100*, 9242.
- (86) Schlienz, H.; Beckendorf, M.; Katter, U.J.; Risse, T.; Freund, H-J. *Phys. Rev. Lett.* **1995**, *74*, 761.
- (87) Stoll, S.; Schweiger, A. *J. Magn. Reson.* **2006**, *178*, 42.
- (88) Walsh, A. D. *J. Chem. Soc.* **1953**, 2260.
- (89) March, N.H. *J. Chem. Phys.* **1981**, *74*, 2973.
- (90) Frisch, M. J.; et al. Gaussian 03, Revision C.02, Gaussian, Inc., Wallingford CT, 2004.
- (91) Chiesa, M.; Paganini, M.C.; Giamello, E.; Murphy, D.M.; Di Valentin, C.; Pacchioni, G. *Acc. Chem. Res.* **2006**, *39*, 861 and references therein.
- (92) Goldsborough, J.P.; Koehler, T.R. *Phys. Rev.* **1964**, *133A*, 135.
- (93) Chiesa, M.; Giamello, E.; Di Valentin, C.; Pacchioni, G.; Sojka, Z.; Van Doorslaer, S. *J. Am. Chem. Soc.* **2005**, *127*, 16935.
- (94) Catterall, R.; Edwards, P.P. *J. Phys. Chem.* **1980**, *84*, 1196.
- (95) Lian, J.C.; Finazzi, E.; Di Valentin, C.; Gao, H.-J.; Risse, T.; Pacchioni, G.; Freund, H.-J. *Chem. Phys. Lett.* **2008**, *450*, 308.
- (96) Catterall, R.; Edwards, P.P. *Chem. Phys. Lett.* **1976**, *42*, 540.
- (97) Catterall, R.; Edwards, P.P. *Chem. Phys. Lett.*, **1976**, *43*, 122.
- (98) Finazzi, E.; Di Valentin, C.; Pacchioni, G.; Chiesa, M.; Giamello, E.; Gao, H.; Lian, J.; Risse, T.; Freund, H-J. *Chem. Eur. J.* **2008**, *14*, 4404.
- (99) Yulikov, M.; Sterrer, M.; Heyde, M.; Rust, H.P.; Risse, T.; Freund, H-J.; Pacchioni, G., Scagnelli, A. *Phys. Rev. Lett.* **2006**, *96*, 146804-4.
- (100) Chenier, J.H.B.; Howard, J.A.; Joly, H.A.; Mile, B. *J. Chem. Soc. Faraday Trans.* **1990**, *86*, 2169.
- (101) Olm, M.T.; Symons, M.C.R.; Eachus, R.S. *Proc. R. Soc. London, Ser. A* **1984**, *392*, 227.
- (102) Holmberg, G.E.; Unruh, W.P.; Friauf, R.J. *Phys. Rev. B* **1976**, *13*, 983.
- (103) Chiesa, M.; Napoli, F.; Giamello, E. *J. Phys. Chem C* **2007**, *111*, 5481.
- (104) *CO₂ Utilisation for Global Sustainability*, Park E.S.; Clay J. S.; Lee, K.W., Eds; Elsevier: Amsterdam, 2004.
- (105) Lunsford, J.H.; Jayne, J.P. *J. Phys. Chem.* **1965**, *69*, 2182.
- (106) Naccache, C., *Chem. Phys. Lett.* **1971**, *11*, 323.
- (107) Huzimura, R.; Kurisu, H.; Okuda, T. *Surf. Sci.* **1988**, *197*, 444.
- (108) Meriaudeau, P.; Vadrine, J.C.; Ben Taarit, Y.; Naccache, C. *J. Chem. Soc., Faraday Trans. II* **1975**, *71*, 736.
- (109) Chiesa, M.; Giamello, E. *Chem. Eur. J.* **2007**, *13*, 1261.
- (110) Preda, G.; Pacchioni, G.; Chiesa, M.; Giamello, E. *J. Phys. Chem. C* **2008**, *112*, 19568.
-
- (111) D. W. Ovenall, D. H. Whiffen, *Mol. Phys.* **1961**, *4*, 135.
- (112) Schlick, S.; Silver, B.L.; Luz, Z. *J. Chem. Phys.* **1971**, *54*, 867.
- (113) Ogata, A.; Kazusaka, A.; Enyo, M. *J. Phys. Chem.* **1986**, *90*, 5201.
- (114) Lunsford, J. H.; Jayne, J. P. *J. Phys. Chem.* **1966**, *44*, 1492.

- (115) Morris, R.M.; Kaba, K.A.; Groshens, T.G.; Klabunde K.J.; Baltisberger, R.J.; Woolsey, N.F.; Stenberg, V.I. *J. Am. Chem. Soc.* **1980**, *102*, 3419.
- (116) Cordischi, D.; Indovina, V.; Occhiuzzi, M. *J. Chem. Soc. Faraday Trans. I* **1980**, *76*, 1147.
- (117) Morris, R. M.; Klabunde, K. J. *J. Am. Chem. Soc.* **1983**, *105*, 2633.
- (118) Cordischi, D.; Indovina, V. *Stud. Surf. Sci. Catal.* **1980**, *76*, 1147.
- (119) Giamello, E.; Murphy, D.; Marchese, L.; Martra, G.; Zecchina, A. *J. Chem. Soc. Faraday Trans. I* **1993**, *89*, 3715.
- (120) Olivella, S.; Pericas, M. A.; Serratos, F.; Messegner, A. *J. Mol. Struct.*, **1983**, *105*, 91.
- (121) Ferrari, A.M.; Pacchioni, G. *J. Chem. Phys.* **1997**, *107*, 2066.
- (122) Zecchina, A.; Coluccia, S.; Spoto, G.; Scarano, D.; Marchese, L. *J. Chem. Soc. Faraday Trans. I* **1990**, *86*, 703.
- (123) Marchese, L.; Coluccia, S.; Martra, G.; Giamello, E.; Zecchina, A. *Materials Chem. Phys.* **1991**, *29*, 437.
- (124) Topchieva, K.V.; Spiridonov, S.E.; Loginov, A.Yu. *Zh. Fizicheskoi Khimii* **1986**, *60*, 411.
- (125) Moon, S. C.; Yamashita, H.; Anpo, M. *Stud. Surf. Sci. Catal.* **1994**, *90*, 479.
- (126) Moens, P.; Callens, F.; Matthys, P.; Maes, F.; Verbeeck, R.; Naessens, D. *J. Chem. Soc., Faraday Trans. I* **1991**, *87*, 3137.
- (127) Moens, P.D.W.; Callens, F.J.; Verbeeck, R.M.H.; Naessens, D.E. *App. Radiat. Isotopes* **1993**, *44*, 279.
- (128) Ben Taarit, Y.; Vadrine J.C.; Naccache C.; de Montgolfier P.; Meriaudeau, P. *J. Chem. Phys.* **1977**, *67*, 2880.
- (129) Schlick, S.; Kevan L.; *J. Chem. Phys.* **1980**, *72*, 784.
- (130) Lipatkina, N.I.; Shubin, V.E.; Shvets, V.A.; Chuvylkin, N.D.; Kazanskii, V.B. *Kinet. Katal.* **1982**, *23*, 670.
- (131) Hochstrasser, G.; Antonini, J. F. *Surf. Sci.* **1972**, *32*, 644.
- (132) Radtsig, V.A, Bystikov, A.V. *Kinet. Katal.* **1978**, *19*, 713.
- (133) Radtsig, V.A. *Kinet. Katal.* **1979**, *20*, 448.
- (134) Radtsig, V.A. *Kinet. Katal.* **1979**, *20*, 1203.
- (135) *Biogeochemical Cycles in Elements*; Sigel, A; Sigel, H; Sigel, R.K.O, Eds.; Marcel Dekker: New York, 2005.
- (136) *Catalytic Ammonia Synthesis. Fundamentals and Practice*; Jennings, R.L. Ed.; Plenum Press: New York, 1991.
- (137) Shelef, M. *Chem Rev.* **1995**, *95*, 209.
- (138) Brailsford, J.R.; Morton J.R.; Vanotti, L.E. *J. Phys. Chem.* **1969**, *50*, 1051.
- (139) Henderson, R.A.; Leigh, G.J.; Pickett, C.J. *Adv. Inorg. Chem. Radiochem.* **1983**, *27*, 197.
- (140) Bazhenova, T.A.; Shilov, A.E. *Coord. Chem. Rev.* **1995**, *144*, 64.
- (141) Kim, J.; Rees, D. C. *Biochemistry*, **1994**, *33*, 389.
- (142) Paganini, M.C.; Chiesa, M.; Giamello, E.; Coluccia, S.; Martra, G.; Murphy, D.M.; Pacchioni, G. *Surf. Sci.* **1999**, *421*, 246.
- (143) Giamello, E.; Murphy, D.M.; Paganini, M.C.; Ferrari, A.M.; Pacchioni G. *J. Phys. Chem. B*, **1997**, *101*, 971.
- (144) Giamello, E.; Chiesa, M.; Murphy, D.M.; Paganini, M.C.; Pacchioni, G.; Soave, R.; Rockenbauer, A. *J. Phys. Chem. B*, **2000**, *104*, 1887.
- (145) Chiesa, M.; Giamello, E.; Murphy, D.M.; Pacchioni, G.; Paganini, M.C.; Soave, R.; Sojka, Z.. *J. Phys. Chem. B* **2001**, *105*, 497.
- (146) Sojka, Z.; Chiesa, M.; Paganini, M.C.; Giamello, E. *Stud. Surf. Sci. Catal.* **2001**, *140*, 413.
- (147) Ferrari, A.M.; Soave, R.; D'Ercole, A.; Pisani, C.; Giamello, E.; Pacchioni, G. *Surf. Sci.* **2001**, *479*, 83.
- (148) Ricci, D.; Pacchioni, G.; Sushko, P.; Shluger, A. *Surf. Sci.* **2003**, *542*, 293.
- (149) Iwamoto, M.; Furukawa, H.; Mine, Y.; Uemura, F.; Mikuriya, S.; Kagawa, S. *J. Chem. Soc. Chem. Commun.* **1986**, 1272.
- (150) Whittaker J.W. *J. Chem. Ed.* **1991**, *68*, 421.
- (151) Lunsford, J. H. *J. Chem. Phys.* **1967**, *46*, 4347.
- (152) Lunsford, J. H. *J. Phys Chem.* **1968**, *72*, 2141.
- (153) Lunsford, J. H. *J. Phys Chem.* **1968**, *72*, 4163.
- (154) Kasai, P.; Bishop, R.J. *J. Am. Chem. Soc.* **1972**, *94*, 5560.
- (155) Kasai, P.H.; Bishop, R. J. In *Zeolite Chemistry and Catalysis*. Rabo, J.A. Ed; ACS Monograph 171, American Chemical Society, Washington, DC 1976.
- (156) Hoffman, B.M.; Nelson, N.J. *J. Chem. Phys.* **1969**, *50*, 2598.
- (157) Yahiro, H.; Lund, A.; Benetis, N.P.; Shiotani, M. *Chem. Lett.* **2000**, *7*, 736.
- (158) Lunsford, J. H. *J. Catal.* **1969**, *14*, 379.
- (159) Primet, M.; Che, M.; Naccache, C.; Mathieu, M.V.; Imelik, B. *J. Chim. Phys.* **1970**, *67*, 1629.
- (160) Martinez-Arias, A.; Soria, J.; Conesa, J.C.; Seoane, X.L.; Arcoya, A.; Cataluna, R. *J. Chem. Soc. Faraday Trans.* **1995**, *91*, 1679.
- (161) Che, M.; Giamello, E. *Stud. Surf. Sci. Catal.* **1990**, *12B*, 265.
- (162) Di Valentin, C.; Pacchioni, G.; Chiesa, M.; Giamello, E.; Abbet S.; Heiz, U. *J. Phys. Chem. B* **2002**, *106*, 1637.
- (163) Rudolf, T.; Pöppl, A.; Hofbauer, W.; Michel, D. *Phys. Chem. Chem. Phys.* **2001**, *3*, 2167.
- (164) Pöppl, A.; Rudolf, T.; Michel, D. *J. Am. Chem. Soc.*, **1998**, *120*, 4879.
- (165) Pöppl, A.; Rudolf, T.; Manikandan, P.; Goldfarb, D. *J. Am. Chem. Soc.*, **2000**, *122*, 10194.

-
- (166) Rudolf, T.; Bohlmann, W.; Pöpl, A. *J. Mag. Res.* **2002**, *155*, 45.
- (167) Volodin, A.; Biglino, D.; Itagaki, I.; Shiotani, M.; Lund, A. *Chem. Phys. Lett.* **2000**, *327*, 165.
- (168) Yahiro, H.; Lund, A.; Aasa, R.; Benetis, N.P.; Shiotani, M. *J. Phys. Chem. A.* **2000**, *104*, 7950.
- (169) Biglino, D.; Bonora, M.; Volodin, A.; Lund, A. *Chem. Phys Lett.* **2001**, *349*, 511.
- (170) Zhang, G.; Tanaka, T.; Yamaguchi, T.; Hattori, H.; Tanabe, K. *J. Phys Chem.* **1990**, *94*, 506.
- (171) Paganini, M.C.; Chiesa, M.; Martino, P.; Giamello, E. *J. Phys. Chem. B.* **2002**, *106*, 12531.
- (172) Che, M.; Naccache C. *Chem. Phys. Lett.* **1971**, *8*, 45.
- (173) Di Valentin, C.; Pacchioni G.; Selloni A.; Livraghi, S.; Giamello, E. *J. Phys. Chem. B*, **2005**, *109*, 11414.
- (174) Enemark, J.H.; Feltham, R. D. *Coord. Chem. Rev.* **1974**, *13*, 339.
- (175) Chiesa, M.; Paganini, M.C.; Giamello, E.; Di Valentin C. ; Pacchioni, G. *J. Mol. Catal. A* **2003**, *204-205*, 779.
- (176) Berlier, G.; Spoto G.; Bordiga, S.; Ricchiardi, G.; Fiscaro, P.; Zecchina, A.; Rossetti, I.; Selli, E.; Forni, L.; Giamello, E.; Lamberti, C. *J. Catal.* **2002**, *208*, 64.
- (177) Fiscaro, P.; Giamello, E.; Berlier, G.; Lamberti, C. *Res. Chem. Intermed.* **2003**, *29*, 805.
- (178) Chao, C.C.; Lunsford, J.H. *J. Phys. Chem.* **1972**, *76*, 1546.
- (179) Naccache, C.; Che, M.; Ben Taarit, Y. *Chem. Phys. Lett.* **1972**, *13*, 109.
- (180) Giamello, E.; Murphy, D.M.; Magnacca, G.; Morterra, C.; Shioya, Y.; Nomura, T.; Anpo, M. *J. Catal.* **1992**, *136*, 510.
- (181) Anpo, M., Nomura, T.; Kitao, T.; Giamello, E.; Murphy, D.M.; Che, M.; Fox, M. A. *Res. Chem. Intermed.* **1991**, *15*, 225.
- (182) Iwamoto, M.; Hamada, H. *Catal. Today* **1991**, *10*, 57.
- (183) Sojka, Z.; Che, M.; Giamello, E. *J. Phys Chem. B.* **1997**, *101*, 4831.
- (184) Poppl, A.; Hartmann, M. *Stud. Surf. Sci. Catal.* **2002**, *142*, 375.
- (185) Umamaheswari, V.; Poppl, A.; Hartmann, M. *J. Mol. Catal. A.* **2004**, *223*, 123.
- (186) Umamaheswari, V.; Hartmann, M.; Poppl, A. *J. Phys. Chem. B.* **2005**, *109*, 19723.
- (187) Neyman, K.M.; Ganyushin, D.I.; Nasluzov, V.A.; Rosch, N.; Poppl, A.; Hartmann, M. *Phys. Chem. Chem. Phys.* **2003**, *5*, 2429.
- (188) Umamaheswari, V.; Hartmann, M.; Poppl, A. *J. Phys. Chem. B.* **2005**, *109*, 10842.
- (189) Naccache, C.; Che, M. In *Proceedings of the 5th International Congress on Catalysis*; Hightower J.W., Ed.; North Holland: Amsterdam 1973.
- (190) Anpo, M.; Aikawa, N.; Kubokawa, Y.; Che, M.; Louis, C.; Giamello, E. *J. Phys Chem.* **1985**, *89*, 5017.
- (191) Nagata, M.; Yahiro, H.; Shiotani, M.; Lindgren, M.; Lund, A.; *Chem. Phys. Lett.* **1996**, *256*, 27.
- (192) Lunsford, J. H. *J. Colloid. Interf. Sci.* **1968**, *26*, 355.
- (193) Garrone, E.; Guglielminotti, E.; Zecchina, A.; Giamello, E. *J. Chem. Soc. Faraday Trans.* **1984**, *80*, 2723.
- (194) Garrone, E.; Giamello, E. *Stud. Surf. Sci. Catal.* **1985**, *21*, 225.
- (195) Ugliengo, P.; Garrone, E. Giamello, E. *Zeit. Physik..Chem.* **1987**, *152*, 31.
- (196) Kolosov, A.K.; Shvets, V.A; Chuvylki, N.D.; Kazansky V. B. *J. Catal.* **1977**, *47*, 190.
- (197) Schoonheydt, R. A.; Lunsford, J. H. *J. Phys Chem.* **1972**, *76*, 323.
- (198) Atkins, P.W.; Horsfield, A.; Symons, M.C.R. *J. Chem. Soc.* **1964**, 5220.
- (199) Dinse, K.P.; Möbius, K. *Z. Naturforsch. A.* **1968**, *23*, 695.
- (200) Mashchenko, A.I.; Pariiskii, G.B.; Kazanskii, V.B. *Kinet. Katal.* **1968**, *9*, 151.
- (201) Ben Taarit Y.; Naccache, C.; Che, M.; Tench, A.J. *Chem. Phys Lett.* **1974**, *24*, 41.
- (202) Lin, M.J.; Lunsford, J.H. *J. Phys Chem.* **1976**, *80*, 635.
- (203) Lunsford, J.H.; Johnson, D.P. *J. Chem. Phys.* **1973**, *58*, 2079.
- (204) Lin, M.J.; Johnson, D.P.; Lunsford, J.H. *Chem. Phys Lett.* **1972**, *15*, 412.
- (205) Lin, M.J.; Lunsford, J.H. *J. Phys Chem.* **1976**, *80*, 2015
- (206) Livraghi, S., Paganini, M.C., Chiesa, M., Giamello, E. *Res. Chem. Intermed.* **2006**, *32*, 777.
- (207) Coope, J.A.R.; Gardner, C.L.; McDowell, C.A.; Pelman, A.I. *Mol. Phys.* **1971**, *21*, 1043.
- (208) Castner, T.G.; Känzig, W. *J. Phys Chem. Solids* **1957**, *3*, 178.
- (209) Raghunathan P.; Sur S.K. *J. Am. Chem. Soc.* **1984**, *106*, 8014.